$SCF^{\beta\text{-}TRCP}$ suppresses angiogenesis and thyroid cancer cell migration by promoting ubiquitination and destruction of VEGF receptor 2

Shavali Shaik,[1] Carmelo Nucera,[1,2] Hiroyuki Inuzuka,[1] Daming Gao,[1] Maija Garnaas,[4,5] Gregory Frechette,[1] Lauren Harris,[1] Lixin Wan,[1] Hidefumi Fukushima,[1] Amjad Husain,[1,2] Vania Nose,[7] Guido Fadda,[8] Peter M. Sadow,[3] Wolfram Goessling,[4,5,6,9] Trista North,[1,9] Jack Lawler,[1,2] and Wenyi Wei[1]

[1]Division of Cancer Biology and Angiogenesis, Department of Pathology, and [2]Center for Vascular Biology Research, Beth Israel Deaconess Medical Center, [3]Department of Pathology, Endocrine Service, Massachusetts General Hospital, [4]Division of Genetics and [5]Division of Gastroenterology, Hepatology and Endoscopy, Brigham and Women's Hospital, and [6]Gastrointestinal Cancer Center, Dana-Farber Cancer Institute, Harvard Medical School, Boston, MA 02215
[7]Department of Pathology, Miller School of Medicine, University of Miami, Miami, FL 33136
[8]Endocrine Pathology, Catholic University Policlinico A. Gemelli, Rome 00168, Italy
[9]Harvard Stem Cell Institute, Harvard University, Cambridge, MA 02138

The incidence of human papillary thyroid cancer (PTC) is increasing and an aggressive subtype of this disease is resistant to treatment with vascular endothelial growth factor receptor 2 (VEGFR2) inhibitor. VEGFR2 promotes angiogenesis by triggering endothelial cell proliferation and migration. However, the molecular mechanisms governing VEGFR2 stability in vivo remain unknown. Additionally, whether VEGFR2 influences PTC cell migration is not clear. We show that the ubiquitin E3 ligase $SCF^{\beta\text{-}TRCP}$ promotes ubiquitination and destruction of VEGFR2 in a casein kinase I (CKI)–dependent manner. β-TRCP knockdown or CKI inhibition causes accumulation of VEGFR2, resulting in increased activity of signaling pathways downstream of VEGFR2. β-TRCP–depleted endothelial cells exhibit enhanced migration and angiogenesis in vitro. Furthermore, β-TRCP knockdown increased angiogenesis and vessel branching in zebrafish. Importantly, we found an inverse correlation between β-TRCP protein levels and angiogenesis in PTC. We also show that β-TRCP inhibits cell migration and decreases sensitivity to the VEGFR2 inhibitor sorafenib in poorly differentiated PTC cells. These results provide a new biomarker that may aid a rational use of tyrosine kinase inhibitors to treat refractory PTC.

CORRESPONDENCE
Wenyi Wei:
wwei2@bidmc.harvard.edu

Abbreviations used: ATC, anaplastic thyroid cancer; CHX, cycloheximide; CKI, casein kinase I; EV, empty vector; FTC, follicular thyroid cancer; HMVEC, human microvascular endothelial cell; MO, morpholino; PTC, papillary thyroid cancer; TKI, tyrosine kinase inhibitor; VEGF, vascular endothelial growth factor; VEGFR2, VEGF receptor 2; WCL, whole cell lysate.

Angiogenesis, the process of new blood vessel formation from existing vessels, plays an important role in normal physiology (Tonnesen et al., 2000), as well as in many pathological conditions including cancer (Folkman, 1971; Papetti and Herman, 2002), macular degeneration (Ahmad et al., 2011), and various vascular diseases (Khurana et al., 2005). Strikingly, increased angiogenesis is observed in many types of human cancers (Bergers and Benjamin, 2003; Dvorak, 2003), whereas angiogenesis is decreased in age-associated vascular diseases (Ungvari et al., 2010). Therefore, diseases that are associated with increased angiogenesis, such as human cancers, can be treated by inhibiting angiogenesis (Folkman, 2007). In contrast, stimulation of angiogenesis could be beneficial in the treatment of coronary artery disease and other vascular diseases characterized by insufficient blood flow to target organs as a result of blocked or damaged blood vessels (Khan et al., 2002; Al Sabti, 2007). Many factors that influence

S. Shaik, C. Nucera, and H. Inuzuka contributed equally to this paper.

The Rockefeller University Press $30.00
J. Exp. Med. 2012 Vol. 209 No. 7 1289-1307
www.jem.org/cgi/doi/10.1084/jem.20112446

The Journal of Experimental Medicine

angiogenesis have been identified; however, the molecular mechanisms by which angiogenesis is regulated are still not fully understood. Therefore, identifying the mechanisms that regulate blood vessel formation would be beneficial in treating various diseases associated with angiogenesis defects.

Vascular endothelial growth factor (VEGF) is one of the most potent proangiogenic growth factors involved in the regulation of angiogenesis (Brown et al., 1997; Ferrara, 1999). Although there are three types of VEGF receptors, VEGF receptor 2 (VEGFR2; also named KDR or Flk1) is the principal receptor that transmits VEGF-A signals in vascular endothelial cells, which subsequently results in enhanced angiogenesis (Shibuya and Claesson-Welsh, 2006). The critical role of VEGFR2 in vascular development is highlighted by the fact that *VEGFR2*$^{-/-}$ mice die at embryonic days 8.5–9.5 (E8.5–9.5) as a result of defective development of endothelial cells and blood islands (Shalaby et al., 1995). Recent studies revealed that VEGFR2 also plays a major role in tumor angiogenesis as well as in tumor growth (Fong et al., 1999). Moreover, VEGF-A is also secreted by a variety of human and rodent tumor cell lines (Senger et al., 1983, 1986), and VEGFR2 is overexpressed in many cancers including colon (Takahashi et al., 1995), gastric (Zhang et al., 2002), lung (Seto et al., 2006), breast (Kranz et al., 1999), and thyroid cancer (Bunone et al., 1999; Vieira et al., 2005; Rodríguez-Antona et al., 2010). These expression patterns of VEGFR2 and VEGF-A suggest the existence of both paracrine and autocrine signaling between tumor cells and vascular endothelial cells, which contribute to pathological angiogenesis and tumor growth (Alitalo and Carmeliet, 2002; Shibuya and Claesson-Welsh, 2006).

Although elevated levels of VEGFR2 are detected in thyroid tumors (Vieira et al., 2005; Rodríguez-Antona et al., 2010), the molecular mechanisms for such elevation and its contribution to the development of thyroid tumor, whose incidence is increasing more rapidly than other types of human cancers around the world (Leenhardt et al., 2004; Davies and Welch, 2006), still remain largely unknown. Interestingly, the VEGFR2 inhibitor sorafenib, a multi–tyrosine kinase inhibitor (TKI), has been recently used in clinical trials as an anti–thyroid tumor therapy (Cohen et al., 2008; Gupta-Abramson et al., 2008; Kloos et al., 2009; Sherman, 2011). However, the molecular mechanism underlying the usage of sorafenib to treat thyroid tumors, as well as the critical contribution of VEGFR2 in thyroid tumors, remains largely unknown. Moreover, recent clinical trials with sorafenib in patients with aggressive/metastatic forms of thyroid cancers showed only a partial response rate, suggesting that these aggressive tumors may elicit unknown resistance mechanisms to this drug (Gupta-Abramson et al., 2008; Cabanillas et al., 2010). Therefore, identifying the molecular mechanisms by which VEGFR2 is regulated in both endothelial cells and cancer cells will shed new light on how physiological angiogenesis is regulated and how dysfunction in these pathways leads to pathological angiogenesis and tumorigenesis. This knowledge will guide the clinical application of TKIs to a more targeted subgroup of patients to efficiently suppress thyroid tumor growth, migration, and angiogenesis through inhibiting VEGFR2 functions.

Ubiquitin-mediated proteolysis plays an important role in the regulation of many cellular processes by facilitating the timely destruction of key regulatory proteins by the 26S proteasome complex (Ciechanover et al., 2000). SCF$^{\beta\text{-TRCP}}$ is a well characterized E3 ubiquitin ligase that is involved in the degradation of many proteins involved in cell signaling and cell cycle regulation (Liu et al., 1999; Busino et al., 2003; Watanabe et al., 2004). Furthermore, β-TRCP, a substrate recognition subunit of SCF$^{\beta\text{-TRCP}}$, has a prominent role in breast cancer, as it regulates prolactin receptor levels in a proteasome-dependent manner (Li et al., 2006). This type of ligand-stimulated receptor degradation is one of the mechanisms that are involved in negative regulation of several growth factor receptors, including EGFR, PDGFR, and CSFR1, which belong to the family of receptor tyrosine kinase (Schlessinger, 2000). This degradation process is mainly initiated by the addition of ubiquitin moieties after receptor engagement, which then targets the ubiquitinated receptors to the lysosomal/proteasomal machineries for proteolysis. It has been reported that the carboxyl terminus of VEGFR2 is required for ligand-dependent activation of VEGFR2 signaling as well as PKC-mediated down-regulation of VEGFR2 (Meyer et al., 2004; Singh et al., 2005). A recent study indicated the involvement of a PEST motif in the down-regulation of VEGFR2 protein (Meyer et al., 2011). However, the molecular mechanisms of VEGFR2 degradation, as well as the significance of this pathway in controlling angiogenesis in vivo, still remain unknown. Here we report that the SCF$^{\beta\text{-TRCP}}$ E3 ligase plays a key role in regulating angiogenesis, through modulating VEGFR2 stability and the activities of VEGFR2 downstream signaling pathways. Our results also offer the molecular understanding and the rationale for targeted use of sorafenib to treat thyroid cancer patients with relatively low β-TRCP protein expression levels.

RESULTS

VEGFR2 stability is controlled by β-TRCP

Multi-subunit Cullin–Ring complexes comprise the largest known class of E3 ubiquitin ligases (Petroski and Deshaies, 2005). Cullins directly interact with Roc1, a Ring finger protein, and the Cullin–Roc1 complex comprises the core module of a series of E3 ubiquitin ligases. Thus, we started our investigation by examining whether a specific Cullin–Ring complex interacts with VEGFR2. We found that Cullin 1, but not other members of the Cullin family that we examined, specifically interacts with VEGFR2 (Fig. 1, A and B). This suggests that the SCF complex, which contains Cullin 1, might be involved in the regulation of VEGFR2 stability. In keeping with this notion, depletion of endogenous Cullin 1, but not Cullin 4A, resulted in the up-regulation of VEGFR2 expression in human microvascular endothelial cells (HMVECs; Fig. 1 C). Next, we sought to explore which F-box protein, when complexed with Cullin 1, is responsible for VEGFR2

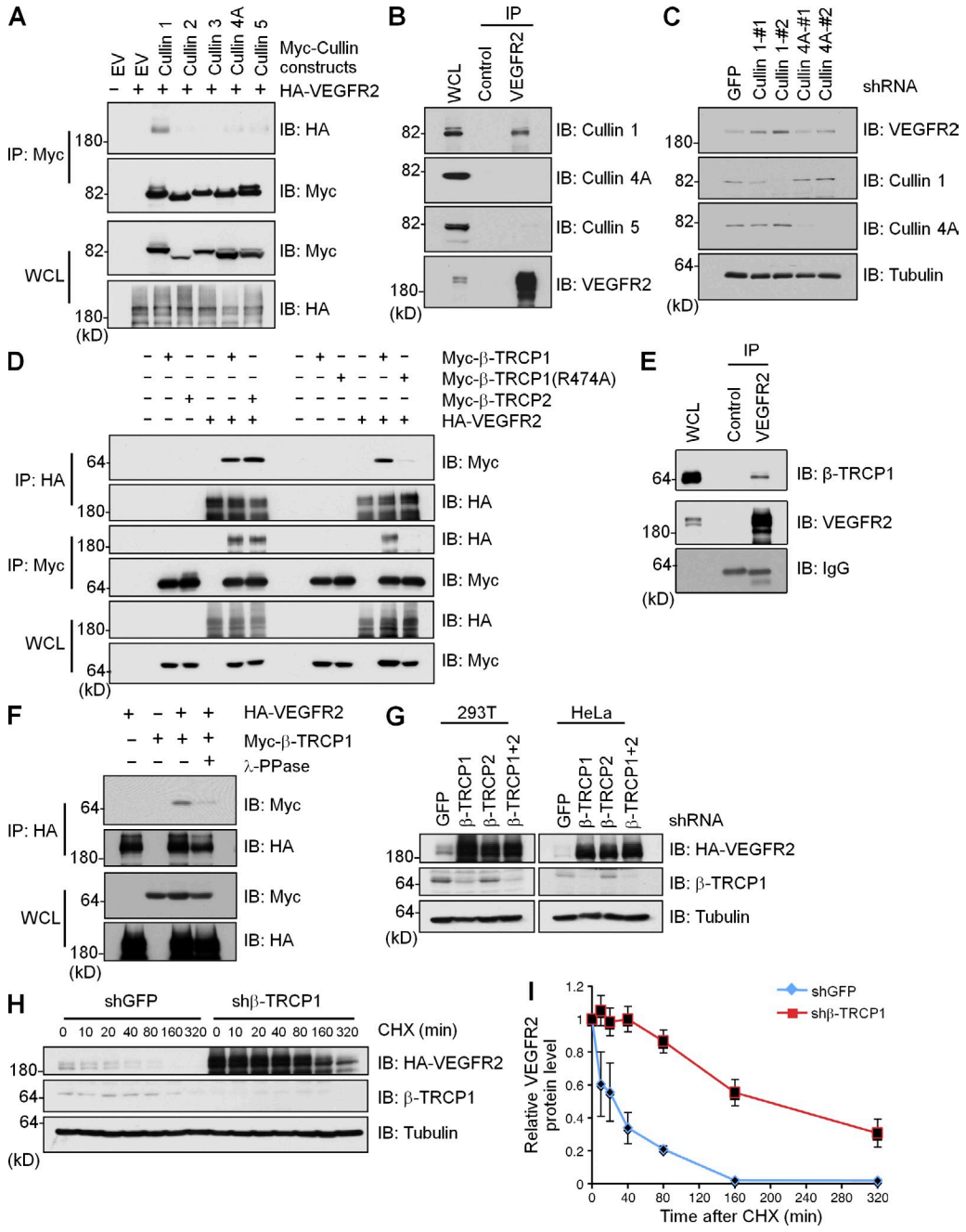

Figure 1. VEGFR2 stability is controlled by SCF$^{\beta\text{-TRCP}}$. (A) Immunoblot analysis of WCLs and immunoprecipitates (IP) derived from 293T cells transfected with HA-VEGFR2 and various Myc-tagged Cullin constructs or EV. Data shown is representative of two independent experiments. (B) Immunoblot analysis of HMVEC WCLs and anti-VEGFR2 immunoprecipitates. Mouse IgG was used as a negative control for the immunoprecipitation procedure. Data shown is representative of two independent experiments. (C) Immunoblot analysis of HMVECs infected with the shRNA constructs specific for GFP or the indicated Cullin constructs. Data shown is representative of two independent experiments. (D) Immunoblot analysis of immunoprecipitates and WCL derived from 293T cells transfected with HA-VEGFR2 and/or Myc-tagged β-TRCP1, β-TRCP2, or β-TRCP1 (R474A) constructs. Data shown is representative of two independent experiments. (E) Immunoblot analysis of HMVEC WCLs and anti-VEGFR2 immunoprecipitates. Mouse IgG was used as a negative control for the immunoprecipitation procedure. Data shown is representative of two independent experiments. (F) Immunoblot analysis of WCL and immunoprecipitates derived from 293T cells transfected with HA-VEGFR2 and Myc–β-TRCP1 constructs as indicated. Where indicated, cell lysates were pretreated with λ-phosphatase before the immunoprecipitation procedure. Data shown is representative of two independent experiments. (G) Immunoblot analysis of WCL from 293T and HeLa cells transfected with shRNA constructs specific for GFP or β-TRCP1, β-TRCP2, or β-TRCP1+2. Data shown is representative of two independent experiments. (H) 293T cells were transfected with the indicated shRNA constructs. 20 h after transfection, cells were split into 60-mm dishes. 20 h later, cells were treated with 20 µg/ml CHX. At the indicated time points, WCLs were prepared, and immunoblots were probed with the indicated antibodies. Data shown is representative of three independent experiments. (I) Quantification of the band intensities in H. VEGFR2 band intensity was normalized to tubulin, and then normalized to the t = 0 controls. The error bars represent mean ± SD (n = 3).

degradation. β-TRCP, one of the well characterized F-box proteins, binds to its substrates by recognizing a specific DSG(XX)S phosphodegron motif, within which the two serine residues are phosphorylated (Frescas and Pagano, 2008). We noticed that the cytoplasmic tail of VEGFR2 contains three DSG(XX)S motifs that could potentially be recognized by β-TRCP and are conserved among different species (see Fig. 3 A). This prompted us to examine whether β-TRCP interacts with VEGFR2 in vitro. Using coimmunoprecipitation, we found that both β-TRCP1 and β-TRCP2 interact with VEGFR2 (Fig. 1 D). The interaction between VEGFR2 and β-TRCP1 was abolished when the C-terminal WD40 repeat motif of β-TRCP1, which has been shown to mediate the interaction with most of its substrates (Wu et al., 2003), was mutated (Fig.1 D). Furthermore, we detected an interaction between endogenous VEGFR2 and endogenous β-TRCP1 in HMVECs (Fig. 1 E) and further demonstrated that phosphatase treatment abolished the interaction between VEGFR2 and β-TRCP1 (Fig. 1 F). In support of an important role for β-TRCP in regulating VEGFR2 abundance, depletion of either β-TRCP1 or β-TRCP2 led to up-regulation of VEGFR2 levels (Fig. 1 G). More importantly, depletion of β-TRCP did not affect significantly VEGFR2 mRNA levels (see Fig. 4 D), suggesting that the observed increase in VEGFR2 abundance was mainly through posttranscriptional mechanisms. In support of this notion, using cycloheximide, we demonstrated that the half-life of VEGFR2 was markedly extended after depletion of β-TRCP1 (Fig. 1, H and I).

Casein kinase I (CKI) is involved in the regulation of VEGFR2 protein stability

It has been demonstrated that β-TRCP substrates need to be phosphorylated within their degron sequences by specific kinases before their recognition and destruction by the $SCF^{\beta\text{-TRCP}}$ complex (Jin et al., 2003; Cardozo and Pagano, 2004). We therefore sought to identify the upstream kinase that phosphorylates VEGFR2 and triggers its destruction. To this end, we transfected 293T cells with HA-VEGFR2 and Flag–β-TRCP1, along with different kinases (CKIδ [Inuzuka et al., 2010] and GSK3β [Liu et al., 2002]) that have been previously identified to play a critical role in facilitating β-TRCP–mediated proteolysis of the target protein. CKIδ, but not GSK3β, promoted the destruction of ectopically expressed VEGFR2 (Fig. 2 A). Furthermore, this degradation of VEGFR2 was completely blocked when treated with the proteasome inhibitor MG132, suggesting the involvement of 26S proteasome (Fig. 2 A). Importantly, the R474A mutant form of β-TRCP1 that is impaired to interact with VEGFR2 (Fig. 1 D) failed to promote VEGFR2 destruction by CKIδ (Fig. 2 B), suggesting a critical role of β-TRCP1 in CKIδ-mediated destruction of VEGFR2.

In further support of a direct role of CKI in VEGFR2 protein stability, VEGFR2 levels were markedly up-regulated in a concentration-dependent manner when HMVECs were treated with D4476, a specific CKI inhibitor (Fig. 2, C and D). Furthermore, coimmunoprecipitation analysis revealed that CKIδ, but not CKIα or CKIε isoforms, specifically interacts with VEGFR2 (Fig. 2 E). Consistent with this finding, depletion of endogenous CKIδ, but not other CKI isoforms (CKIα and CKIε), led to a significant increase in endogenous VEGFR2 abundance (Fig. 2 F). Consistent with a negative role of CKIδ in VEGFR2 stability control, depletion of CKIδ significantly extended endogenous VEGFR2 half-life in HMVECs (Fig. 2, G and H). In a reciprocal set of experiments, we found that overexpression of CKIδ markedly decreased the half-life of VEGFR2 (Fig. 2 I).

CKIδ phosphorylates VEGFR2 at both DSG and DDTD phosphodegrons to promote its interaction with β-TRCP1

Most β-TRCP substrates contain one or several DSG(XX)S degrons that are recognized by β-TRCP when they are properly phosphorylated by one or more kinases (Frescas and Pagano, 2008). We noticed that there are three DSG(XX)S degrons present in the C-terminal tail of VEGFR2 that are conserved among different species (Fig. 3 A; and Fig. S1, A–C). Interestingly, most of the Ser/Thr sites within the putative degrons are predicted to be CKI sites (Fig. S1, E and F). To test the significance of each putative phosphodegron, we created individual point mutations in the DSG motifs by replacing both serine residues with alanine to examine whether these mutants resist CKI-mediated VEGFR2 degradation (Fig. 3 A). We found that individual mutation of each DSG motif (labeled DSG1, DSG2, and DSG3) had no significant effect on β-TRCP–mediated destruction of VEGFR2 in the presence of CKIδ (Fig. 3 B), suggesting that the phosphorylation of all three DSG degrons might be involved in the degradation of VEGFR2. To test this hypothesis, we generated a DSG triple mutant that contains serine to alanine substitutions in all three DSG degrons (labeled as DSG-T). However, VEGFR2–DSG-T could still be degraded by β-TRCP1/CKIδ with similar efficiency (Fig. 3 E). Furthermore, the half-life of DSG-T was not significantly increased in response to VEGF-A (unpublished data), indicating that there are other potential degrons present in VEGFR2 mediating its destruction. Using the ScanSite program, we identified another potential CKI phosphorylation site (DDTD) in the C-terminal tail of VEGFR2 (Fig. 3 A and Fig. S1 F). Thus, we generated additional VEGFR2 mutants (Fig. 3 A) to evaluate the contribution of the DDTD site in β-TRCP–mediated VEGFR2 destruction. Using in vitro kinase assays, we showed that the three identified DSG sites, as well as the newly identified DDTD site, are the major CKI phosphorylation sites. Combinational inactivation of the three DSG degrons (DSG-T), or DDTD alone, significantly reduced CKI-mediated phosphorylation of VEGFR2 (Fig. 3 C). Moreover, combinational mutation of all four putative degrons (9A) further decreased CKI-mediated in vitro phosphorylation of GST-VEGFR2 (Fig. 3 C). Consistent with this result, CKI treatment triggered the interaction between GST-VEGFR2 and β-TRCP1 in vitro (Fig. 3 D). In contrast, mutation of the three putative DSG degrons (DSG-T) led to a reduced interaction between GST-VEGFR2 and β-TRCP1. Interestingly, mutation of all four degrons (9A) led to further reduction in detectable

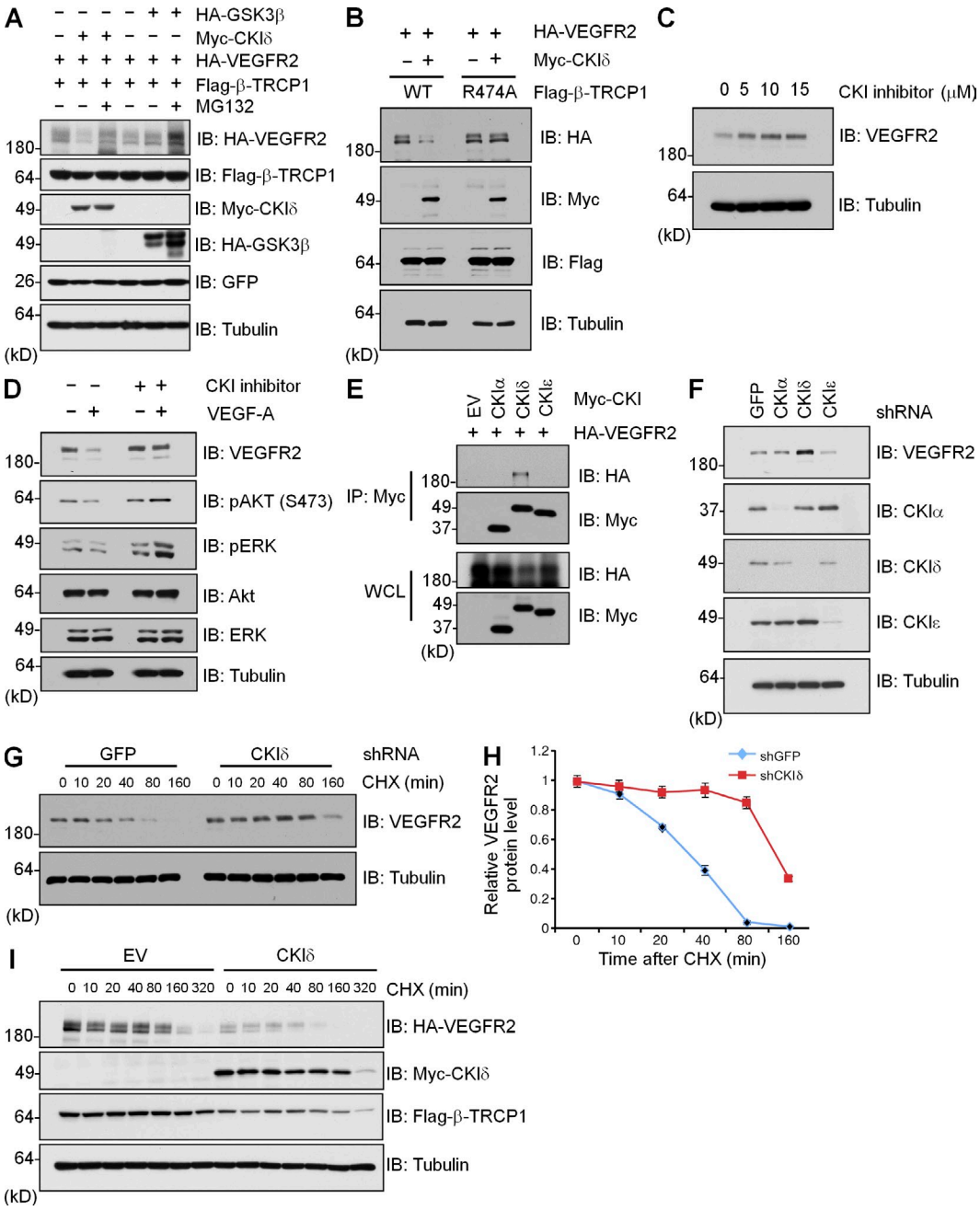

Figure 2. CKI is involved in the regulation of VEGFR2 stability. (A) Immunoblot analysis of 293T cells transfected with HA-VEGFR2, Flag–β-TRCP1, and indicated kinases. Where indicated, cells were treated with the proteasome inhibitor MG132. Data shown is representative of two independent experiments. (B) Immunoblot analysis of 293T cells transfected with HA-VEGFR2 and/or Myc-CKIδ together with Flag-WT–β-TRCP1 or Flag-R474A–β-TRCP1. Data shown is representative of two independent experiments. (C and D) Immunoblot analysis of HMVECs treated with the CKI inhibitor D4476 at the indicated concentrations for 12 h. In D, where indicated, 100 ng/ml VEGF-A was added for 2 h before harvesting. Data shown is representative of two independent experiments. (E) Immunoblot analysis of WCLs and immunoprecipitates (IP) derived from 293T cells transfected with HA-VEGFR2 and Myc-tagged versions of indicated CKI isoforms. Data shown is representative of two independent experiments. (F) Immunoblot analysis of HMVECs infected with shRNA specific for GFP or the indicated CKI isoforms. Data shown is representative of two independent experiments. (G) HMVECs were transfected with the indicated shRNA constructs. 40 h after infection, cells were treated with 1 μg/ml puromycin for 72 h to eliminate the noninfected cells. Afterward, the resulting cells were split into 60-mm dishes and, after another 20 h, were treated with 20 μg/ml CHX. At the indicated time points, WCLs were prepared, and immunoblots were probed with the indicated antibodies. Data shown is representative of three independent experiments. (H) Quantification of the band intensities in G. VEGFR2 band intensity was normalized to tubulin, and then normalized to the t = 0 controls. The error bars represent mean ± SD (n = 3). (I) 293T cells were transfected with EV or a construct encoding CKIδ. 20 h after transfection, cells were split into 60-mm dishes, and after another 20 h cells were treated with 20 μg/ml CHX. At the indicated time points, WCLs were prepared, and immunoblots were probed with the indicated antibodies. Data shown is representative of two independent experiments.

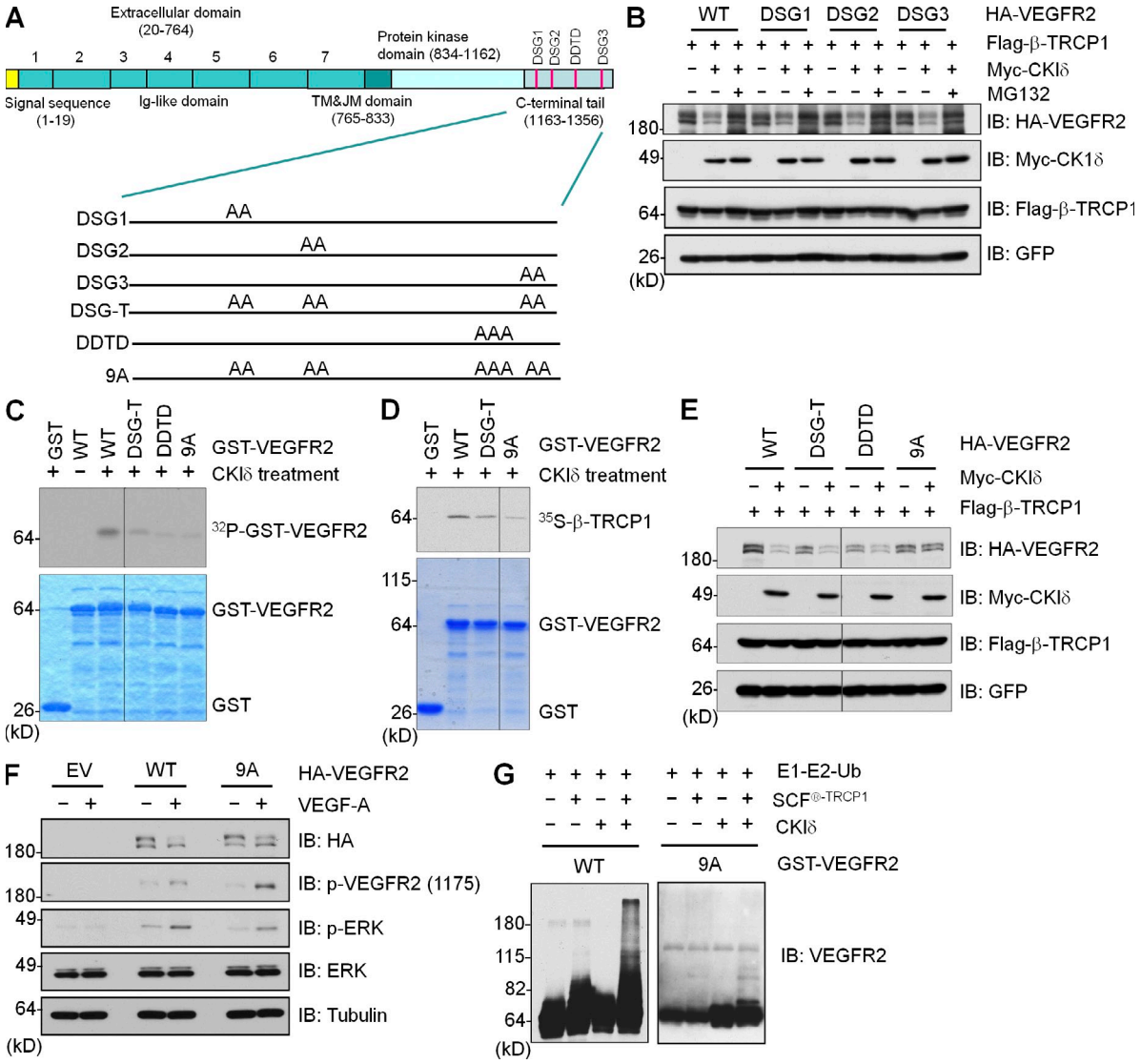

Figure 3. Phosphorylation of VEGFR2 by CKI at multiple sites triggers its ubiquitination and degradation by $SCF^{\beta\text{-}TRCP}$. (A) Illustration of VEGFR2 protein and various VEGFR2 mutants generated for this study. There are three DSG degrons present in the C-terminal tail of VEGFR2 that can be identified by β-TRCP1. AA represents two alanines substituted from two serines in DSG1, DSG2, and DSG3 degrons (Fig. S1, A–C). AAA represents three alanines substituted from three threonines in the DDTD degron (Fig. S1 D). (B) Immunoblot analysis of 293T cells transfected with the indicated HA-VEGFR2 and Flag–β-TRCP1 plasmids in the presence or absence of Myc-CKIδ. Where indicated, cells were treated with the proteasome inhibitor MG132. Data shown is representative of two independent experiments. (C) Purified CKIδ protein was incubated with 5 µg of the indicated glutathione S-transferase (GST)–VEGFR2 fusion proteins in the presence of γ-[^{32}P]ATP. The protein kinase reaction products were resolved by SDS-PAGE, and phosphorylation was detected by autoradiography. Top: autoradiogram of phosphorylated GST-VEGFR2; bottom panel: staining of GST-VEGFR2 to demonstrate equal loading. Data shown is representative of two independent experiments. Black lines indicate that intervening lanes were spliced out. (D) Autoradiograms show a recovery of ^{35}S-labeled β-TRCP1 protein bound to the indicated GST-VEGFR2 fusion proteins (GST protein as a negative control) incubated with CKIδ before pulldown assays. Top: autoradiogram of β-TRCP1 bound with GST-VEGFR2; bottom: staining of GST-VEGFR2 to demonstrate equal loading. Data shown is representative of two independent experiments. Black lines indicate that intervening lanes were spliced out. (E) Immunoblot analysis of 293T cells transfected with the indicated HA-VEGFR2 and Flag–β-TRCP1 plasmids in the presence or absence of Myc-CKIδ. Data shown is representative of two independent experiments. (F) Immunoblot analysis of WCL from 293 cells transfected with indicated constructs. Where indicated, cells were treated with 100 ng/ml VEGF-A for 2 h before harvesting. Data shown is representative of two independent experiments. (G) Affinity-purified $SCF^{\beta\text{-}TRCP}$ complexes were incubated with purified recombinant GST-VEGFR2 proteins, purified E1 and E2, and ubiquitin as indicated at 30°C for 45 min. The ubiquitination reaction products were resolved by SDS-PAGE and probed with the anti-VEGFR2 antibody. Data shown is representative of two independent experiments.

interaction between GST-VEGFR2 and β-TRCP1 (Fig. 3 D), which reflects their deficiency in CKI-mediated phosphorylation (Fig. 3 C). Moreover, consistent with their decreased interactions with β-TRCP1, these mutants are also deficient in β-TRCP1/CKI–mediated proteolysis (Fig. 3 E). Importantly, compared with WT-VEGFR2, 9A-VEGFR2 could

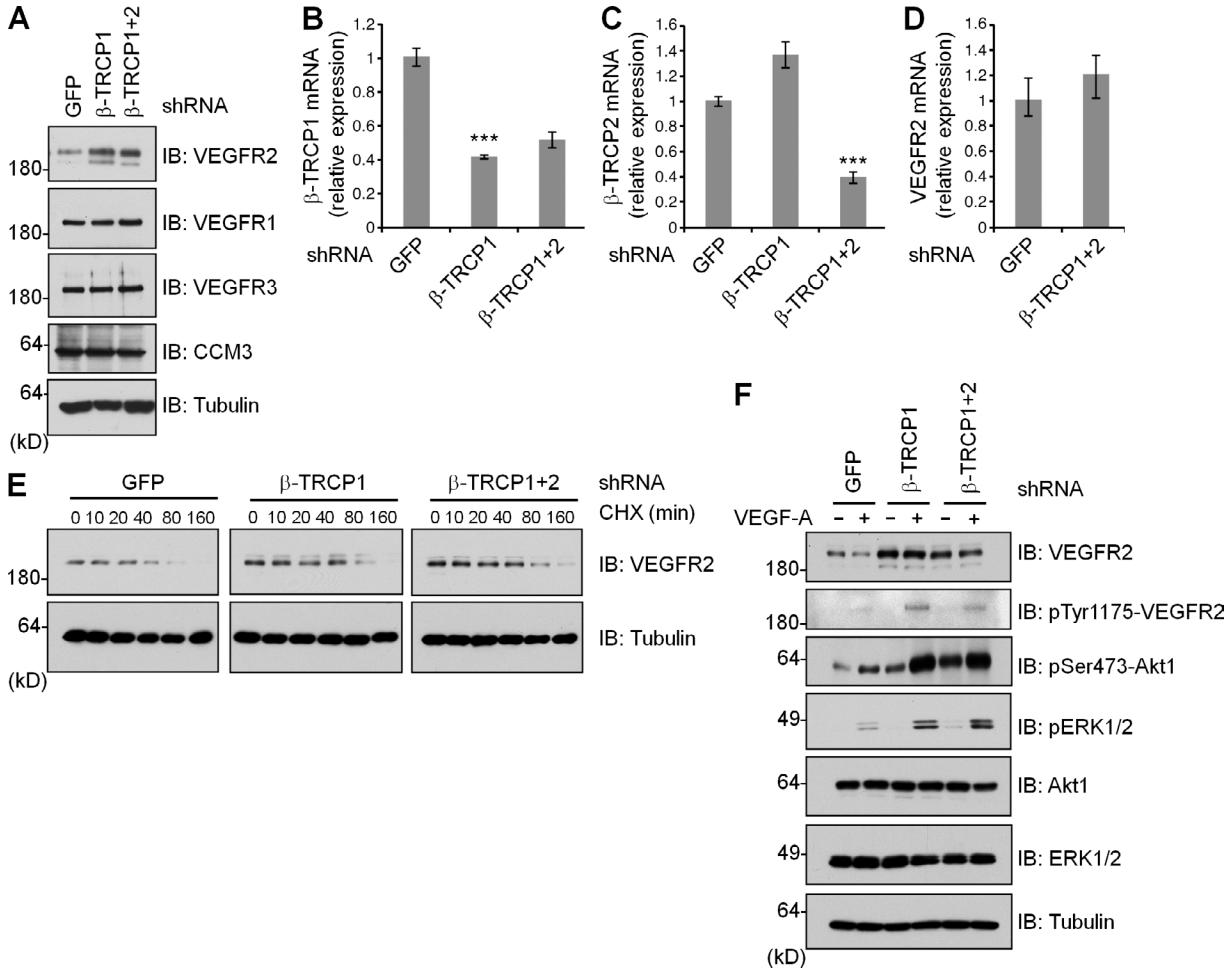

Figure 4. β-TRCP regulates VEGFR2 protein levels in HMVECs. (A) Immunoblot analysis of HMVECs stably expressing lentiviral vectors encoding shRNA specific for GFP, β-TRCP1, and β-TRCP1+2. Data shown is representative of two independent experiments. (B and C) Real-time RT-PCR analysis of β-TRCP1 (B) and β-TRCP2 (C) mRNA expression in HMVECs infected with the indicated shRNA lentiviral vectors. Error bars indicate mean ± SD from three independent experiments. ***, $P < 0.001$. (D) Real-time RT-PCR analysis of VEGFR2 mRNA expression in HMVECs infected with the indicated shRNA lentiviral vectors. Error bars indicate mean ± SD from three independent experiments. (E) HMVECs were infected with the indicated shRNA lentiviral vectors. After selection with 1 µg/ml puromycin for 72 h, cells were split into 60-mm dishes and, after another 20 h, treated with 20 µg/ml CHX. At the indicated time points, WCLs were prepared, and immunoblots were probed with the indicated antibodies. Data shown is representative of three independent experiments. (F) Immunoblot analysis of the HMVECs shown in A, stimulated where indicated with 100 ng/ml VEGF-A for 15 min. Data shown is representative of two independent experiments.

similarly activate the downstream ERK signaling pathway (Fig. 3 F) and promote cell migration in a VEGF-A–dependent manner (unpublished data), indicating that 9A-VEGFR2 is functional in vivo. We further showed that β-TRCP1 promotes in vitro VEGFR2 ubiquitination in a CKI-dependent manner (Fig. 3 G) and that the inefficient destruction of 9A-VEGFR2 observed in Fig. 3 E is likely a result of deficient ubiquitination of VEGFR2 (Fig. 3 G).

Depletion of β-TRCP increases VEGFR2 protein levels, VEGF-A–induced signaling, cell migration, and enhanced tube formation in HMVECs

Because VEGFR2 is predominantly expressed in endothelial cells and is involved in the regulation of angiogenesis, we next investigated whether depletion of endogenous β-TRCP affects VEGFR2 protein abundance in HMVECs under physiological conditions. Depletion of either β-TRCP1 or β-TRCP1+2 in HMVECs (Fig. 4, B and C) led to up-regulation of VEGFR2 protein levels (Fig. 4 A). In contrast, depletion of endogenous β-TRCP did not affect the expression of other VEGF receptors (VEGFR1 and VEGFR3) or CCM3, a protein recently reported to modulate VEGFR2 function (Fig. 4 A; He et al., 2010). Furthermore, β-TRCP depletion did not affect cell viability compared with shGFP control cells (unpublished data). These results suggest that β-TRCP might regulate angiogenesis through specifically targeting VEGFR2 for ubiquitination and destruction. Furthermore, β-TRCP depletion did not cause a marked change in VEGFR2 mRNA levels (Fig. 4 D), suggesting that β-TRCP regulates VEGFR2 expression mainly through a

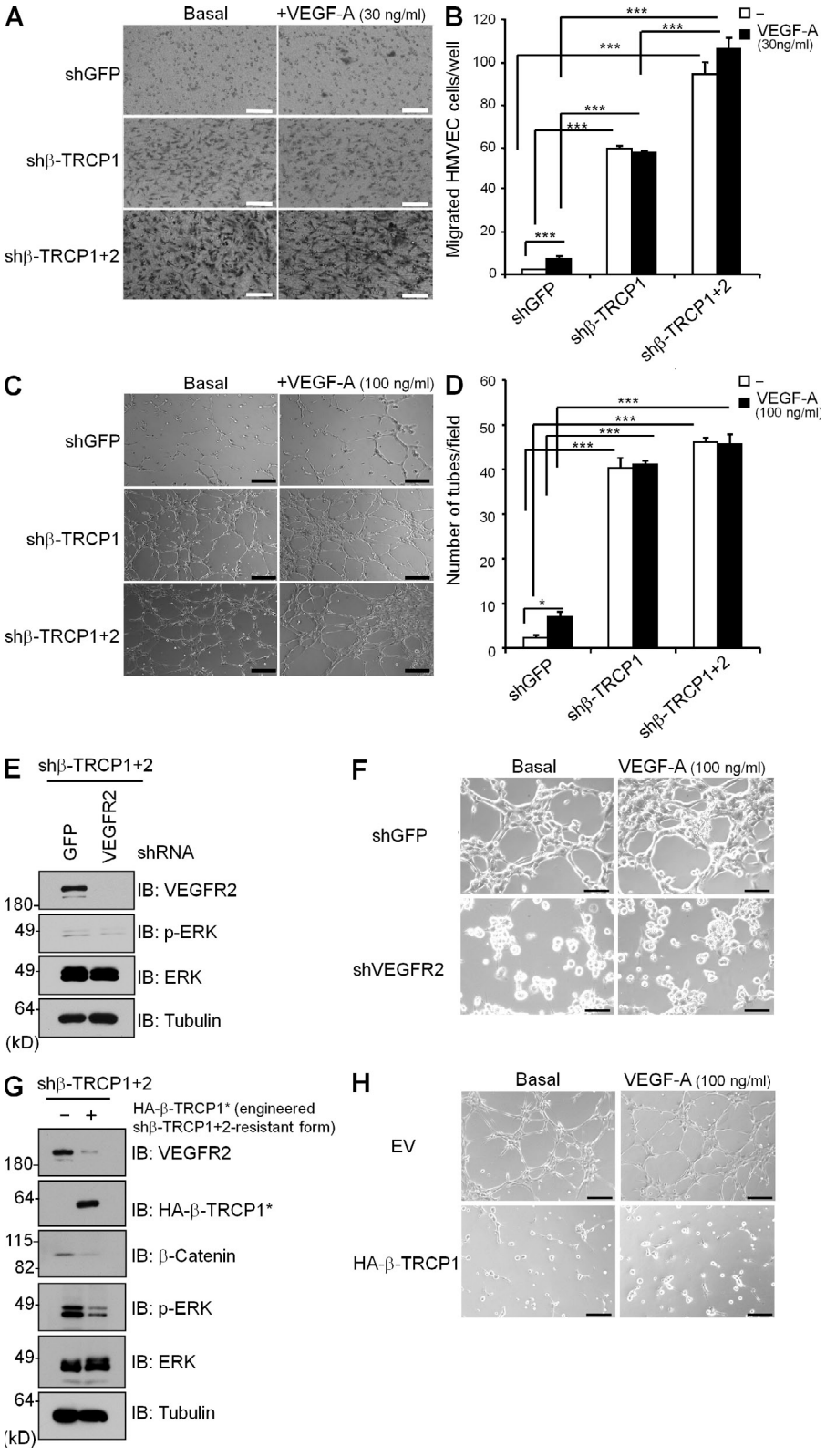

Figure 5. β-TRCP regulates endothelial cell migration and angiogenesis in vitro. (A) HMVECs were exposed to 30 ng/ml VEGF-A where indicated. Recruited cells were photographed after 5 h. Bars, 10 µm. Data shown is representative of three independent experiments. (B) Quantitative measurement of cell migration shown in A. The error bars represent mean ± SD. ***, $P < 0.001$; $n = 3$. (C) HMVECs shown in A were subjected to a Matrigel tube formation assay in the presence or absence of 100 ng/ml VEGF-A and photographed after 5 h. Bars, 10 µm. Data shown is representative of three independent experiments. (D) Quantitative measurement of tubes formed in C. The error bars represent mean ± SD. *, $P < 0.05$; ***, $P < 0.001$; $n = 3$. (E) Immunoblot analysis of the HMVECs infected with the indicated shRNA lentiviral vectors. Data shown is representative of two independent experiments. (F) HMVECs shown in E were exposed to 100 ng/ml VEGF-A where indicated. Recruited cells were photographed after 5 h. Bars, 10 µm. Data shown is representative of two independent experiments. (G) Immunoblot analysis of the HMVECs infected with HA-β-TRCP1 where indicated. Data shown is representative of two independent experiments. (H) HMVECs shown in G were subjected to a Matrigel tube formation assay in the presence or absence of 100 ng/ml VEGF-A and photographed after 5 h. Bars, 10 µm. Data shown is representative of two independent experiments.

posttranscriptional mechanism. Consistently, the half-life of endogenous VEGFR2 was increased in β-TRCP–depleted HMVECs compared with shGFP-treated cells (Fig. 4 E). More importantly, we found that depletion of β-TRCP results in increased activity of VEGFR2 downstream signaling pathways as indicated by increased p-VEGFR2 (pTyr1175), p-AKT (pSer473), and p-ERK1/2 levels (Fig. 4 F; Shibuya and Claesson-Welsh, 2006).

Consistent with the role of β-TRCP in regulating VEGFR2 abundance and the activities of downstream signaling pathways, compared with shGFP-treated HMVECs, β-TRCP–depleted HMVECs exhibited increased migration (Fig. 5, A and B). Furthermore, using in vitro angiogenesis (matrigel tube formation) assays, we found that depletion of endogenous β-TRCP in HMVECs leads to a significant increase in their capacity to form tubes as compared with control cells infected with shGFP (Fig. 5, C and D). VEGF-A addition significantly increased the number of tubes in shGFP cells;

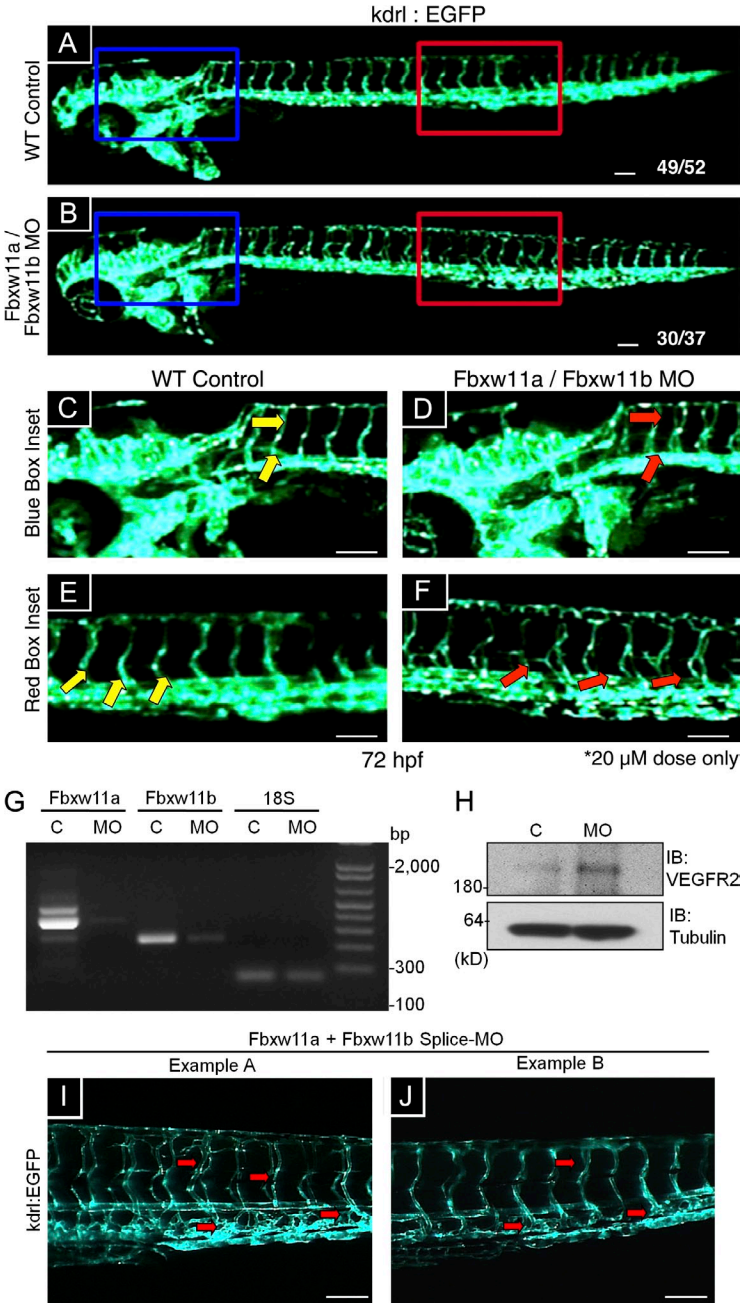

Figure 6. Inactivation of β-TRCP2 leads to VEGFR2 up-regulation and increased angiogenesis in zebrafish in vivo. (A and B) Vascular development in control (A) or 20 μM MO (B)-treated KdrI:EGFP embryos. MO was used to deplete both Fbxw11a and Fbxw11b. Images were taken by fluorescence microscopy at 72 h postfertilization (hpf). Bars, 50 μm. Data shown is representative of three independent experiments. (C and D) Close-up images of blood vessel formation in the head/anterior trunk of zebrafish treated with control (C corresponds to the blue-boxed regions of A) or Fbxw11a and Fbxw11b MOs (D corresponds to the blue-boxed regions of B). Yellow arrows in C point to junction areas where normal mirror-paired intersomitic vessel development was observed, whereas red arrows in D point to areas of excess/disorganized branching of intersomitic vessels. Bars, 50 μm. Data shown is representative of three independent experiments. (E and F) Close-up images of blood vessel formation in the posterior trunk/tail of zebrafish treated with control (E corresponds to the red-boxed regions of A) or Fbxw11a and Fbxw11b MOs (F corresponds to the red-boxed regions of B). Yellow arrows in E point to junction areas where normal mirror-paired intersomitic vessel development was observed, whereas red arrows in F point to areas of excess/disorganized branching of intersomitic vessels. Bars, 50 μm. Data shown is representative of three independent experiments. (G) RT-PCR analysis of endogenous Fbxw11a and Fbxw11b mRNA levels in MO-treated zebrafish compared with sibling controls (C). Data shown is representative of three independent experiments. (H) VEGFR2 protein expression was analyzed by Western blot in control (C) and β-TRCP2–MO-treated zebrafish embryos. Data shown is representative of two independent experiments. (I and J) Close-up images of blood vessel formation in the red-boxed region in the posterior trunk/tail of zebrafish treated with combination treatment of splice MO against Fbxw11a and Fbxw11b. Red arrows point to areas of excess/ disorganized branching of intersomitic vessels observed after depletion of both Fbxw11a and Fbxw11b. Bars, 50 μm. Data are representative of three independent experiments.

however, VEGF-A addition did not increase the number of tubes either by shβ-TRCP1 or shβ-TRCP1+2 cells (Fig. 5, C and D), suggesting that because these cells already have increased ability to form tubes, further addition of VEGF-A did not increase tube formation in shβ-TRCP cells. Furthermore, additional depletion of VEGFR2 blocked the elevated tube formation in β-TRCP–depleted HMVECs, indicating that VEGFR2 may be the major route through which β-TRCP regulates the tube formation ability of HMVECs (Fig. 5, E and F), while reintroducing β-TRCP into the β-TRCP–depleted HMVECs retarded their in vitro tube formation (Fig. 5, G and H). These results therefore indicate a causal relationship between loss of β-TRCP and elevated in vitro tube formation in HMVECs.

Because both enhanced cellular migration and elevated in vitro tube formation are positive markers for increased angiogenesis, these results support a potential role for β-TRCP in regulating the angiogenesis process through modulating VEGFR2 stability. However, we recognize that the in vitro cell-based assays may not accurately model the angiogenesis process under physiological conditions. To obtain direct evidence to support the potential role of β-TRCP in regulation of angiogenesis, we used a well characterized in vivo zebrafish model (Nasevicius et al., 2000; Habeck et al., 2002) to evaluate how β-TRCP governs VEGFR2 stability to influence angiogenesis.

β-TRCP2 depletion leads to increased expression of VEGFR2 and in vivo angiogenesis in zebrafish

It has been previously demonstrated that both VEGF-A and VEGFR2 are required for vasculogenesis in zebrafish (Nasevicius et al., 2000; Habeck et al., 2002). Loss of VEGF-A function

severely affects the formation of the entire vasculature, whereas VEGFR2 dysfunction impairs the formation of blood vessels generated by sprouting (Nasevicius et al., 2000; Habeck et al., 2002). Thus, we sought to examine whether inactivation of β-TRCP by morpholino (MO) treatment affects vasculogenesis and/or angiogenesis in zebrafish. Interestingly, zebrafish does not contain a homologue of human β-TRCP1 but contains two paralogues of β-TRCP2 (called Fbxw11a and Fbxw11b). Embryos injected with control or MOs specifically inactivating Fbxw11a or Fbxw11b alone or in combination were monitored for alterations in blood vessel formation over 72 h after fertilization. Although a small dose-dependent decrease of embryo viability was observed with either the Fbxw11a or Fbxw11b MO alone, at the highest concentration (100 µM) injected, >90% of the zebrafish embryos were still viable (Fig. S2). In contrast, combinatorial MO injection significantly reduced embryo viability, such that at a concentration of 100 µM, 100% lethality was observed. Combinatorial low-dose MO injection (20 µM) resulted in reduced viability compared with controls (61.5%) but allowed the embryos to develop with overall normal gross morphology allowing analysis (Fig. S2). These data indicate that there is partial functional redundancy between the two β-TRCP2 paralogues.

To further characterize the potential role of β-TRCP2 in angiogenesis, we used the low-dose (20 µM) combinatorial MO strategy to simultaneously inactivate both Fbxw11a and Fbxw11b during zebrafish vascular development in two endothelial reporter lines: Kdrl:EGFP (Fig. 6, A–F; Cross et al., 2003) and fli1a:EGFP (unpublished data; Lawson and Weinstein, 2002). Whereas large blood vessels such as the dorsal aorta appeared to form normally, β-TRCP2–MO-injected embryos exhibited dysregulated vessel formation with increased sprouting as compared with controls (Fig. 6, A and B). Fine analysis of the head/anterior trunk (blue boxed region) and posterior trunk/tail (red boxed region; Fig. 6 C–F) demonstrates that compared with the normal blood vessel formation observed in the control embryos (Fig. 6, C and E, yellow arrows), there is a significant increase in the number of branching blood vessels initiated in β-TRCP2–MO-treated zebrafish (Fig. 6, D and F, red arrows). Significantly, unlike the symmetrical pairs of vessels formed at regular intervals along the somite boundaries in controls, in β-TRCP2–MO-injected embryos vascular sprouts were commonly disorganized, originating at several points along the length of each somite, or with multiple branching connections converging at a single point. These results were confirmed by in situ hybridization (unpublished data), as well as combinatorial splice-blocking MOs, demonstrating the specificity of the effect and significant reduction of gene expression of both Fbxw11a and Fbxw11b RT-PCR (Fig. 6 G) compared with uninjected sibling controls. This elevated blood vessel development was found to correlate with increased expression of VEGFR2 (Fig. 6, H–J) after MO-mediated knockdown of β-TRCP2 (Fig. 6 G), consistent with our in vitro data using HMVECs. However, it was recently reported by Kanarek et al. (2010) that the β-TRCP1/2 double knockout mice are nearly normal, with severe defects in spermatogenesis caused by the stabilization of SNAIL. As the authors used shβ-TRCP2 to knock down endogenous β-TRCP2 in the *β-TRCP1*$^{-/-}$ mice background to achieve the β-TRCP1/2 double knockout phenotype, it is possible that the residual expression of β-TRCP2 allows the *shβ-TRCP2/β-TRCP1*$^{-/-}$ mice to function relatively normally. Further studies are required to explore whether deletion of β-TRCP1 and/or β-TRCP2 in mice also results in abnormalities in angiogenesis and vascular development.

β-TRCP suppresses VEGFR2 abundance to inhibit human thyroid cancer and endothelial cell migration, desensitizing human thyroid cancer cells to sorafenib treatment

Thyroid cancer accounts for up to 95% of primary cancers involving the endocrine system. Papillary thyroid cancer (PTC) is the most common type of thyroid cancer, representing 75–85% of all thyroid cancer cases, and various signaling pathways, such as BRAF and MAPK (i.e., ERK1/2), have been identified as participants in the initiation and progression of human PTC (Khurana et al., 2005; Knauf and Fagin, 2009; Nucera et al., 2009, 2010; Keefe et al., 2010; Liu et al., 2010; Chakravarty et al., 2011). Importantly, as in many other human cancers, VEGFR2-induced angiogenesis was found to play a critical role in thyroid cancer angiogenesis (Keefe et al., 2010; Ringel, 2011). In keeping with this notion, recent clinical trials have proposed VEGFR inhibitors, such as axitinib and sorafenib, as anti-thyroid cancer therapeutics (Cohen et al., 2008; Gupta-Abramson et al., 2008), although the underlying mechanism of their therapeutic effects remains unknown. This prompted us to further examine whether β-TRCP negatively governs VEGFR2 stability in the human thyroid cancer, and furthermore, whether de-regulation of this destruction pathway contributes to the pathological progression of human thyroid cancers. In keeping with our hypothesis, we observed a robust inverse correlation between β-TRCP1 and VEGFR2 protein expression levels in the human thyroid cancer cell lines we examined (Fig. 7, A and B). In contrast to SW1736 and 8505C anaplastic thyroid cancer (ATC)–derived cell lines, or the FTC236 metastatic follicular cancer–derived cell line (Fig. 7, A and B), which display high expression of β-TRCP1, the human BCPAP cell line, a poorly differentiated PTC with squamous metaplasia-derived cell line, has very low β-TRCP1 protein expression and elevated VEGFR2 protein expression levels (Fig. 7 A). In support of this result, we also detected an inverse correlation between β-TRCP1 protein expression levels and angiogenic profile (i.e., CD31 immunoexpression) in an array of poorly or well differentiated human PTC with squamous metaplasia foci (Table S1), which were similar to the initial tumor from which the BCPAP cell line was established (Fig. 7 C). In particular, we found that ∼50% of PTC with squamous metaplasia showed high expression levels (3+) of β-TRCP1, both in the cytoplasm of tumor cells or in the endothelial cells, and low/moderate CD31 (1+/2+) or absent VEGFR2 protein

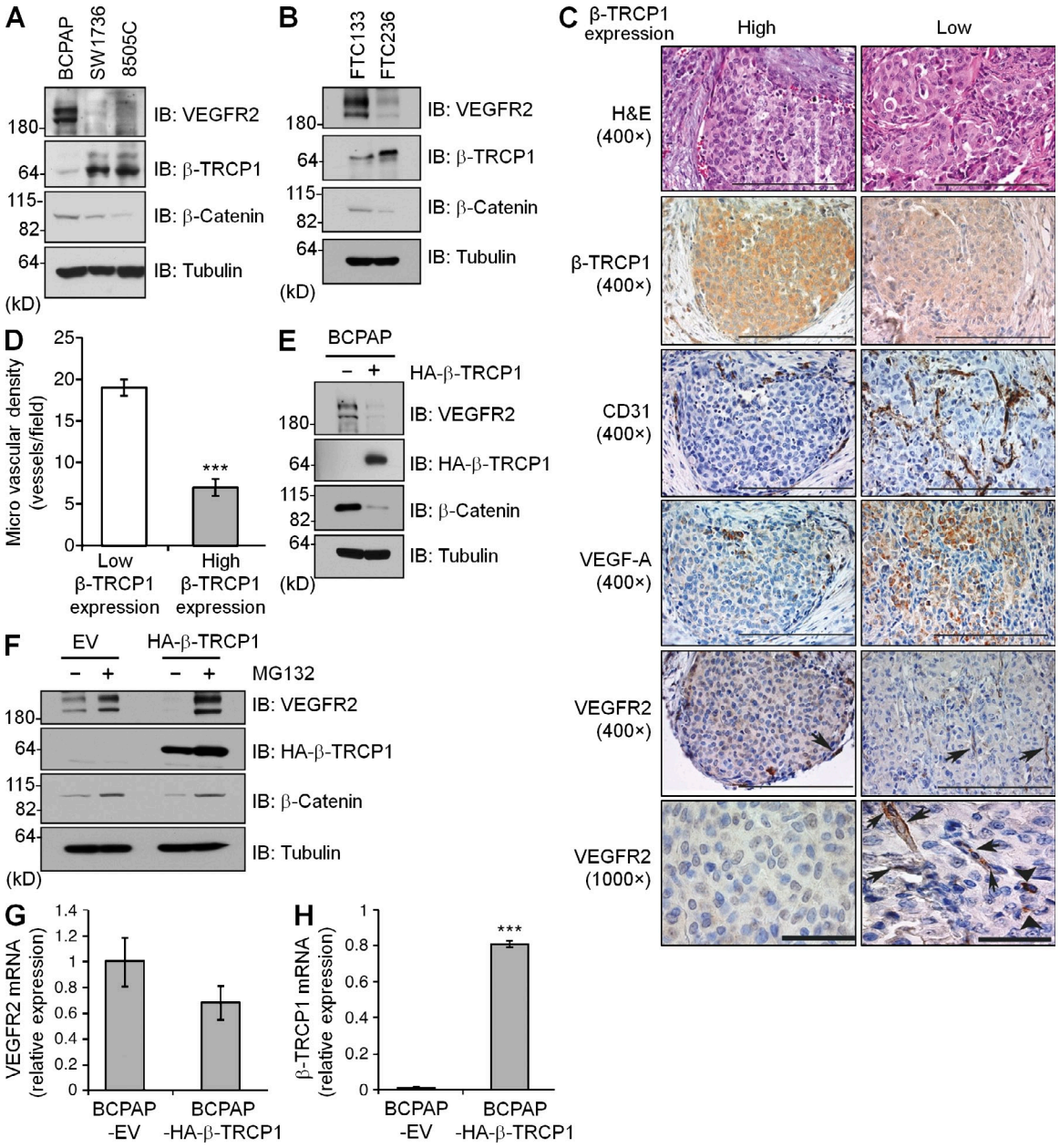

Figure 7. β-TRCP regulates VEGFR2 protein levels in human poorly differentiated PTC-derived cells. (A and B) Immunoblot analysis of various human thyroid cancer cell lines with indicated antibodies. Data are representative of two independent experiments. (C) Human PTC with squamous metaplasia (SM) were stained with the indicated antibodies and analyzed by immunohistochemistry. Low β-TRCP is defined as 1–10% of endothelial or human PTC cells with SM foci being positive for β-TRCP staining. High β-TRCP is defined as >50% of endothelial or human PTC cells with SM being positive for β-TRCP. H+E, H&E staining. Bars: (400×) 200 µm; (1,000×) 50 µm. Arrows and arrowheads highlight endothelium and tumor cells, respectively. (D) Quantitative measurement of the microvascular density (as defined by number of vessels per field showing CD31 staining in PTC samples expressing low or high amounts of β-TRCP1) shown in C. The error bars represent mean ± SD. ***, $P < 0.001$ ($n = 3$). (E and F) Immunoblot analysis of BCPAP cells infected with either EV or HA–β-TRCP1-encoding lentiviral vectors. Where indicated, cells were treated with the proteasome inhibitor MG132. Data are representative of two independent experiments. (G and H) Real-time RT-PCR analysis of VEGFR2 (G) and β-TRCP1 (H) mRNA in BCPAP cells infected with EV or HA-β-TRCP1–encoding lentiviral vectors. Data are representative of three independent experiments. The error bars represent mean ± SD. ***, $P < 0.001$.

expression levels (Fig. 7, C and D). Whereas PTC with low β-TRCP1 protein expression levels (1+) showed increased intratumoral angiogenesis (CD31 immunoexpression; Fig. 7, C and D), and intriguingly ∼6% of PTC cells and 40% of PTC-associated endothelial cells/high-powered fields express VEGFR2 (Fig. 7 C).

Importantly, ectopic expression of β-TRCP1 led to a significant reduction in the endogenous VEGFR2 abundance

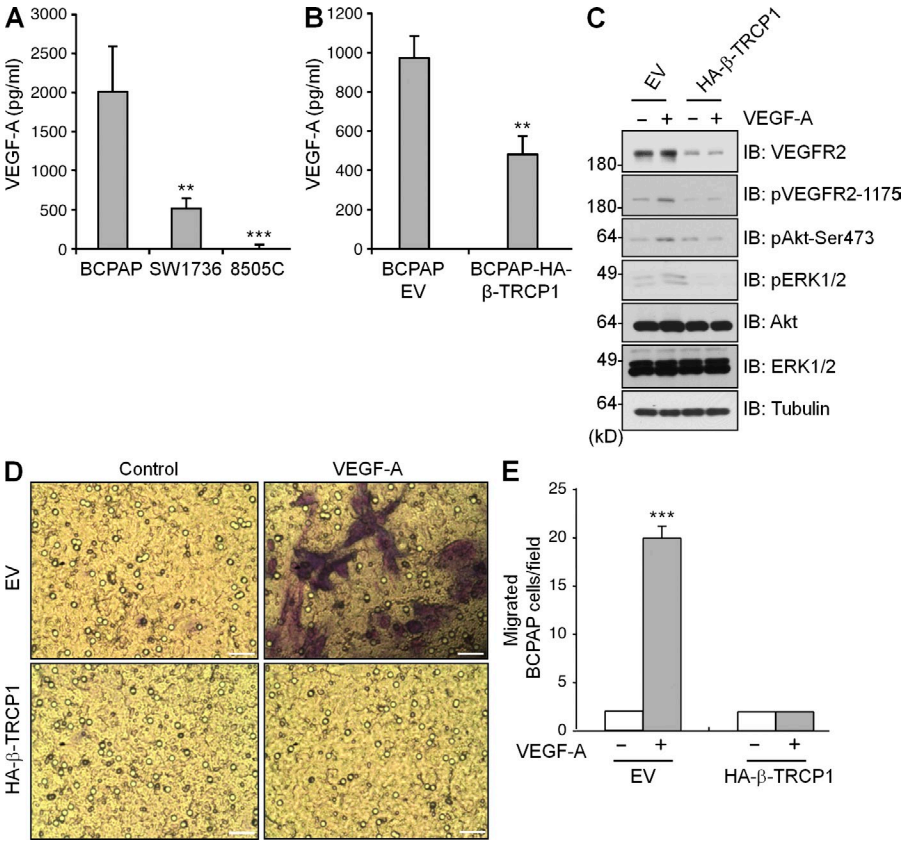

Figure 8. β-TRCP regulates PTC cell migration via regulating VEGFR2 protein levels and VEGF-A secretion in vitro. (A and B) The media from various cultured human thyroid cancer cell lines were collected for ELISA analysis to determine the concentration of secreted VEGF-A. Data are representative of three independent experiments. The error bars represent mean ± SD. **, $P < 0.01$; ***, $P < 0.001$. (C) Immunoblot analysis of BCPAP cells infected with EV or HA–β-TRCP1–encoding lentiviral vectors. Where indicated, VEGF-A was added for 15 min before harvesting. Data are representative of two independent experiments. (D) EV or β-TRCP–expressing BCPAP cells were exposed to 200 ng/ml VEGF-A where indicated. Cells were photographed after 18 h. Bars, 5 µm. Data are representative of three independent experiments. (E) Quantitative measurement of migrated BCPAP cells shown in D. The error bars represent mean ± SD. ***, $P < 0.001$ ($n = 3$).

in the BCPAP cell line (Fig. 7 E) that can be reversed by treatment with the proteasome inhibitor MG132 (Fig. 7 F), arguing that β-TRCP1 is a major negative regulator of VEGFR2 abundance. Furthermore, there was no marked difference in VEGFR2 mRNA levels between empty vector (EV) and β-TRCP1–expressing BCPAP cells, indicating that the regulation of VEGFR2 abundance mainly occurs at the post-transcriptional level (Fig. 7, G and H). These results indicate that in BCPAP (Fig. 7 A) or in poorly differentiated follicular thyroid cancer (FTC)–derived cells (FTC133; Fig. 7 B), β-TRCP1 negatively regulates VEGFR2 abundance, possibly through a ubiquitination-dependent degradation pathway, as it does in human endothelial cells (Fig. 4). Importantly, we found that in human PTC clinical samples there is also a clear inverse correlation between β-TRCP1 expression and several angiogenesis markers (Fig. 7, C and D). This prompted us to further investigate whether elevated VEGFR2 expression in human PTC cells could affect the angiogenesis process of the surrounding endothelial cells.

To this end, we found that the BCPAP with elevated VEGFR2 levels secreted an increased amount of VEGF-A protein (2010 ± 580 pg/ml) compared with the ATC-derived cells SW1736 and 8505C (517 ± 129 and 0.0 pg/ml, respectively) expressing low levels of VEGFR2 (Fig. 8 A), whereas ectopic expression of β-TRCP1 significantly reduced the secreted VEGF-A (470 ± 98 pg/ml in BCPAP-HA-β-TRCP1 cells compared with 967 ± 99 pg/ml in BCPAP-EV cells; Fig. 8 B). Ectopic expression of β-TRCP1 did not affect the mRNA levels of VEGF-A (unpublished data), indicating that β-TRCP1 might regulate VEGF-A through a posttranscriptional mechanism. Whereas additional investigation is warranted to uncover the molecular mechanisms underlying the effect of β-TRCP1 on secretion of VEGF-A, we found that VEGF-A contains an evolutionally conserved DSG-like phosphodegron (Fig. S3), suggesting an interesting possibility that β-TRCP1 may regulate the stability of VEGF-A precursor to indirectly govern its secretion. Importantly, in response to VEGF-A, the downstream signaling pathways of VEGFR2, as detected by the levels of phospho-VEGFR2 (pTyr1175), phospho-Akt (pSer473), and phospho-ERK1/2, are significantly decreased in BCPAP-HA–β-TRCP1 cells compared with BCPAP-EV cells (Fig. 8 C). In a similar fashion to the endothelial cells (Fig. 5, A and B), β-TRCP1–expressing BCPAP cells exhibited significantly less migration in response to VEGF-A compared with the BCPAP-EV cells (Fig. 8, D and E). These results suggested that β-TRCP1 plays a critical role in governing cellular migratory ability, presumably in part via regulating the stability of VEGFR2, in both human endothelial and BCPAP thyroid cancer cell lines.

However, this could not explain why elevated VEGFR2 expression in a subset of human thyroid cancer cells, by itself, could lead to increased angiogenesis which is typically associated with human endothelial cells. To address this question, we used a trans-well system of co-cultured BCPAP cells and human endothelial cells grown in the absence of serum to examine whether manipulation of the β-TRCP1–VEGFR2 signaling pathway in BCPAP cells could affect cellular migration of human endothelial cells (Fig. 9 A). Interestingly, we

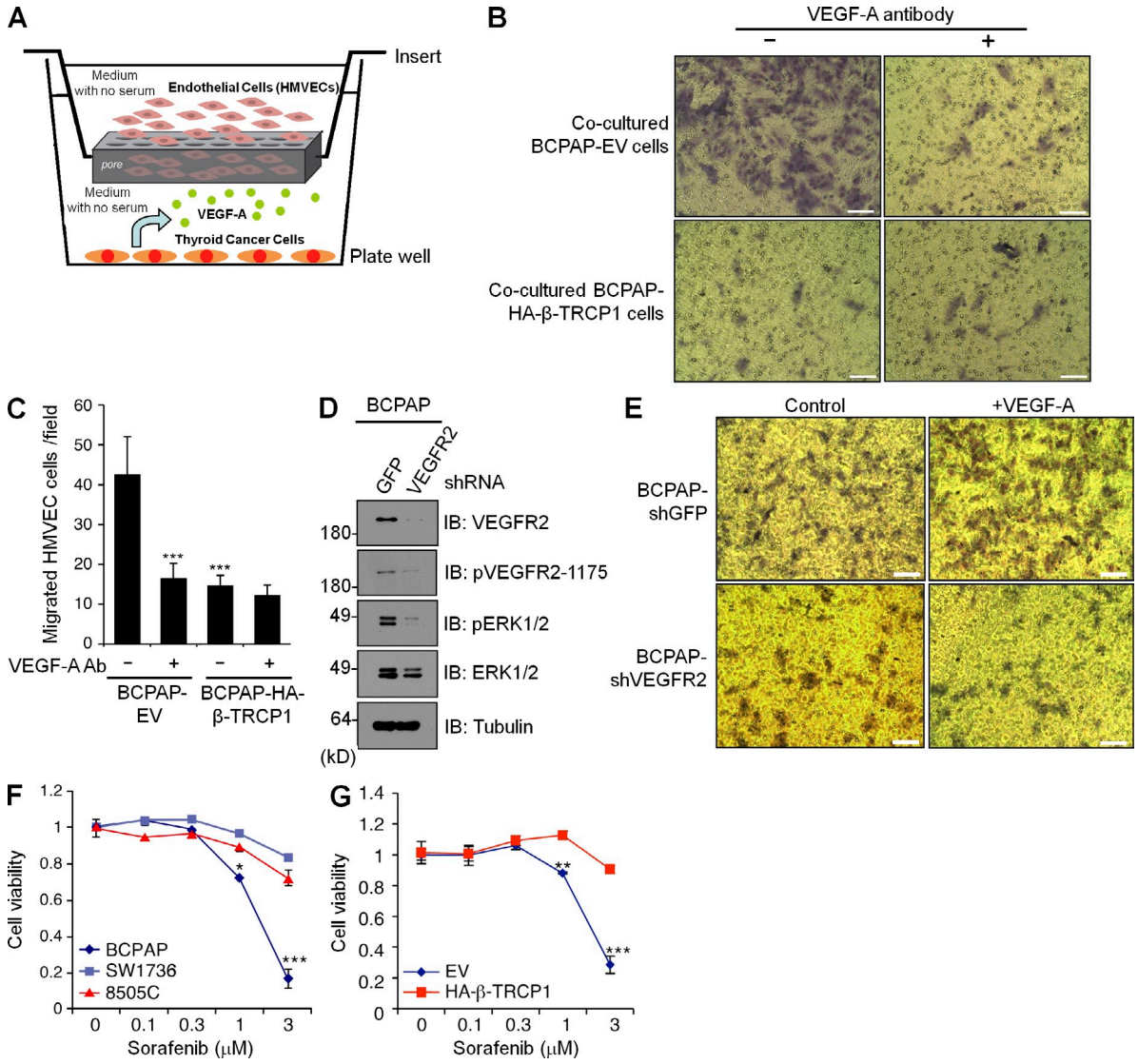

Figure 9. β-TRCP regulates VEGFR2 protein levels in human PTC-derived cells, and thereby influences sensitivity to the VEGFR2 inhibitor sorafenib. (A and B) HMVECs were co-cultured with EV or β-TRCP–expressing BCPAP cells in the presence or absence of VEGF-A antibody. (B) Cells were photographed after 44 h. Bars, 5 µm. Data are representative of three independent experiments. (C) Quantitative measurement of migrated BCPAP cells shown in B. The error bars represent mean ± SD. ***, $P < 0.001$ ($n = 3$). (D) Immunoblot analysis of the BCPAP cells infected with the indicated shRNA lentiviral vectors. Data shown is representative of two independent experiments. (E) BCPAP cells shown in D were exposed to 200 ng/ml VEGF-A where indicated. Recruited cells were photographed after 5 h. Bars, 5 µm. Data shown is representative of two independent experiments. (F) Various PTC cell lines were treated with the indicated concentrations of sorafenib. Cell viability was measured at 48 h. Data shown is representative of three independent experiments. The error bars represent mean ± SD. *, $P < 0.05$; ***, $P < 0.001$ ($n = 3$). (G) EV or HA–β-TRCP1–expressing BCPAP cells were treated with the indicated concentrations of sorafenib. Cell viability was measured at 48 h. The error bars represent mean ± SD. **, $P < 0.01$; ***, $P < 0.001$ ($n = 3$).

found that VEGFR2 levels in BCPAP cells play a critical role in determining migratory ability of the co-cultured HMVECs. Very few HMVECs migrated when they were co-cultured with β-TRCP1–expressing BCPAP cells compared with BCPAP-EV cells (Fig. 9, B and C). This is likely a result of the elevated secretion of VEGF-A from the BCPAP-EV cells because the use of VEGF-A blocking antibody could efficiently abolish cellular migration of the co-cultured HMVECs (Fig. 9, B and C). Furthermore, VEGFR2 knockdown BCPAP (shVEGFR2) cells showed a significant decrease in cell migration compared with control (shGFP) BCPAP cells (Fig. 9, D and E). Overall, these results indicated that elevated VEGFR2 expression in human thyroid cancer cells could not only regulate their own migratory ability via an autocrine mechanism but also regulate the migration of the surrounding human endothelial cells, presumably through a paracrine mechanism. The latter mechanism might offer a possible molecular mechanism for increased VEGFR2 expression that is frequently observed in various human cancers and its correlation with increased angiogenesis.

As recent studies suggest that oncogene addiction could be used as a rationale for targeted anti-cancer therapy (Weinstein and Joe, 2006), we wanted to understand whether expression levels of VEGFR2 in various human thyroid cancer cells correlate with their sensitivity to the VEGFR2 inhibitor, sorafenib. Interestingly, we found that the BCPAP cell line that exhibited increased VEGFR2 protein expression showed increased sensitivity to sorafenib, compared with SW1736 and 8505C ATC-derived cell lines with much lower expression levels of VEGFR2 and corresponding higher levels of β-TRCP1 (Fig. 9 F). At 3 μM sorafenib, the cell viability was significantly decreased in BCPAP cells, whereas no significant decrease was observed in SW1736 and 8505C cells at this sorafenib concentration (Fig. 9 F). Because sorafenib has been proposed as an efficient inhibitor of VEGFR2 kinase, these results indicate that human thyroid cancer cell lines with high levels of VEGFR2, such as BCPAP, might be in part addicted to VEGFR2 activity/functions, and thereby be more sensitive to VEGFR2 inhibitors including sorafenib. Consistent with this notion, we further showed that ectopic expression of β-TRCP1, which efficiently reduced endogenous VEGFR2 levels (Fig. 9 G), could significantly reduce BCPAP's sensitivity to sorafenib. At 3 μM sorafenib concentration, the BCPAP-EV cell viability was significantly reduced when compared with a slight reduction of cell viability in BCPAP-HA–β-TRCP1 cells (Fig. 9 G). Collectively, these results identify a critical role of β-TRCP1 in determining the cellular sensitivity and therapeutic efficacy of sorafenib treatment in human thyroid cancer cells. They further suggest that thyroid cancer patients with low β-TRCP1 expression might respond better to the sorafenib (and maybe to other TKIs) treatment.

DISCUSSION

Here, we show for the first time a possible mechanism by which CKI-dependent phosphorylation of VEGFR2 at specific sites in its C-terminal tail triggers $SCF^{\beta\text{-TRCP}}$-mediated VEGFR2 ubiquitination and destruction. Importantly, our study demonstrated that β-TRCP depletion leads to stabilization of VEGFR2 in human endothelial cells as well as in human thyroid cancer cells, leading to increased sensitivity to VEGF-A–induced stimuli. Correspondingly, this stimuli increased cell migration and enhanced tube formation in β-TRCP–depleted HMVECs. Consistent with the conclusions drawn from our in vitro cell-based assays, we also observed an increased number of branching vessels in zebrafish (Weinstein, 2002) when β-TRCP2 was specifically depleted by MO treatment (Fig. 6, A–F). Moreover, the increased formation of blood vessels was associated with increased VEGFR2 protein levels in β-TRCP2 knockdown zebrafish. These findings indicated a prominent role for β-TRCP in regulating angiogenesis, possibly through the timely destruction of VEGFR2.

Furthermore, we observed a strong inverse correlation between β-TRCP1 and VEGFR2 in BCPAP thyroid cancer cell line (Fabien et al., 1994) as well as in primary PTC with squamous metaplasia (Fig. 7, A and B). For poorly differentiated thyroid cancer patients who fail to respond to the canonical treatment, there is generally neck recurrence and distance metastases leading to low survival rates; thus, rational targeted therapies are needed (Baudin and Schlumberger, 2007). The pathogenesis of squamous transformation of the thyroid gland remains unclear because the gland only contains squamous epithelium under inflammatory processes or neoplasms (Kleer et al., 2000; Walvekar et al., 2006). Furthermore, of the targeted therapies that are used in clinical trials in patients with thyroid cancers, including PTC, sorafenib that targets VEGFR2 signaling has been considered a promising therapeutic intervention (Gupta-Abramson et al., 2008; Lam et al., 2010). However, recent clinical trials based on the use of sorafenib in patients with aggressive/metastatic/progressive thyroid cancers (including PTC or FTCs, etc.) have observed a partial response rate of ∼20% and a stable disease rate of ∼53.3%. Furthermore, patients that histologically had an ATC showed a progressive disease (Gupta-Abramson et al., 2008), indicating that aggressive thyroid cancers may elicit unknown resistance mechanisms to sorafenib.

To this end, we have found for the first time that overexpression of β-TRCP1 markedly depleted VEGFR2 in the BCPAP cells (Fig. 7 E). More importantly, enhanced migration of HMVECs was observed when co-cultured with BCPAP-EV (control) cells. This migration was completely blocked in the presence of antibody to VEGF-A (Fig. 8, D and E), suggesting that the VEGF-A secreted from BCPAP cells induced the HMVEC cell migration. In contrast, the migration of HMVECs was significantly reduced when β-TRCP–overexpressing BCPAP cells were used in the co-cultured/transwell system (Fig. 9, A–C). These results suggested that by altering VEGFR2 and VEGF-A levels, β-TRCP suppresses angiogenesis via a paracrine-mediated mechanism.

Overall, these results pointed to a prominent role for β-TRCP in the negative regulation of VEGFR2 levels in PTC cells. Notably, we also found an inverse correlation between the VEGFR2 expression levels and their pharmacological efficacy/sensitivity to the VEGFR2 inhibitor sorafenib (Fig. 9, F and G). Poorly differentiated human PTC cells with elevated VEGFR2 are more sensitive to sorafenib. Therefore, our results suggest that defects in the β-TRCP/CKI signaling pathway might contribute to increased VEGFR2 protein expression, as well as PTC cell migration and sensitivity to VEGFR2 inhibitor, sorafenib. Furthermore, our work also provides a possible molecular basis for targeted use of VEGFR2 inhibitors, such as sorafenib or other TKIs, to treat more aggressive PTCs refractory to conventional therapies based on β-TRCP expression levels as a novel biomarker. Our results suggest that PTC patients with low expression levels of β-TRCP may respond more favorably to sorafenib treatment, whereas PTC patients with elevated β-TRCP expression might be poor responders. As genomic loss of β-TRCP has been identified in certain types of cancers (Frescas and Pagano, 2008), our results indicate that dysfunction in either β-TRCP or CKI might lead to stabilization of VEGFR2, which could result in hyperactivation of

the VEGF-A–VEGFR2 pathway that facilitates angiogenesis and cancer cell migration.

In summary, our study provides a possible molecular mechanism for the frequent elevation of VEGFR2 displayed in many types of human cancers. Therefore, drugs that activate the β-TRCP and/or CKIδ signaling pathways to induce VEGFR2 destruction could be used to treat various types of human cancers that are associated with increased angiogenesis. In contrast, the identification of both β-TRCP and CKIδ as the upstream components involved in regulating VEGFR2 stability also provides the rationale for developing β-TRCP and CKI inhibitors as potential novel drugs to induce angiogenesis. These pharmacological agents could be used to facilitate new blood vessel formation for the treatment of cardiovascular diseases, such as coronary artery disease or heart injury, that are frequently observed in the aged population.

MATERIALS AND METHODS

Cell culture. HeLa human cervical carcinoma and 293T human embryonic kidney cell lines were cultured in DME medium containing 10% FBS and antibiotics (streptomycin and penicillin). The HMVEC line was cultured in endothelial growth medium (EGM) containing 2% serum and 0.2% bovine brain extract (Shao and Guo, 2004). Human thyroid cancer cell lines: the BCPAP human thyroid cancer cell line harboring the $BRAF^{V600E}$ mutation was established from the primary tumor of a 76-yr-old woman with poorly differentiated PTC with squamous metaplasia (Fabien et al., 1994) and provided by G. Damante (University of Udine, Udine, Italy); and the 8505C human metastatic cell line (human ATC) was purchased from Deutsche Sammlung von Mikroorganismen und Zellkulturen (German collection of microorganisms and cell culture) harboring the $BRAF^{V600E}$ mutation. The human metastatic ATC-derived cell line SW1736 harboring the $BRAF^{V600E}$ mutation was provided by N.E. Heldin (University of Uppsala, Uppsala, Sweden). The FTC133 human FTC-derived cell line and the FTC236 human metastatic FTC-derived cell line were provided by O.H. Clark (University of California, San Francisco Medical Center, San Francisco, CA). BCPAP, FTC133, and FTC236 cells were cultured in DME medium with 10% FBS and antibiotics. SW1736 and 8505C cells were cultured in RPMI medium containing 10% FBS and antibiotics.

Plasmids. pIRES-VEGFR2-HA was obtained from J. Huot and F. Houle (Laval University Cancer Research Center, Quebec, Canada). VEGFR2 mutants were generated with the QuikChange XL Site-Directed Mutagenesis kit (Agilent Technologies) according to the manufacturer's instructions. Various VEGFR2 cDNAs were subcloned using the Pfu polymerase (Agilent Technologies) into the pGEX vector to create GST-VEGFR2 in frame fusion proteins. Short hairpin RNAs (shRNA lentivirus vectors), i.e., shRNA–β-TRCP1, shRNA–β-TRCP1+2, shRNA-GFP, and various CKI constructs were described previously (Jin et al., 2003; Shirogane et al., 2005). Myc–β-TRCP1, Myc–β-TRCP2, Myc–β-TRCP1-R474A, and HA–β-TRCP1 constructs were described previously (Jin et al., 2003; Wu et al., 2003; Shirogane et al., 2005). shβ-TRCP–resistant β-TRCP1 cDNA was described previously (Inuzuka et al., 2010) and was subcloned into Blasticidin-encoding lentiviral vector obtained from Addgene. Myc-Cullin 1, Myc-Cullin 2, Myc-Cullin 3, Myc-Cullin 4A, and Myc-Cullin 5 constructs were gifts from J. DeCaprio (Dana-Farber Cancer Institute, Boston, MA). shRNA constructs against various CKI isoforms were obtained from J. Jin (The University of Texas Health Science Center, Houston, TX). Lentiviral shRNA constructs against GFP and CKIδ were obtained from W. Hahn (Dana-Farber Cancer Institute, Boston, MA). Lentiviral shRNA constructs against VEGFR2 were obtained from Thermo Fisher Scientific, and the specific clone number TRCN0000001687 was used to effectively knock down VEGFR2 in HMVEC and BCPAP cell lines. shRNA lentiviral vectors against Cullin-1 and Cullin-4A were gifts from J. Wade Harper (Harvard Medical School, Boston, MA).

Cell transfections for lentivirus (shRNA) or retrovirus production. 5×10^5 HEK 293T cells were grown in 60-mm plates and transfected using Lipofectamine (Invitrogen) in OptiMEM (Invitrogen) for 48 h according to the manufacturer's instructions. After infection, the cells were selected with 1–2 μg/ml puromycin for 72 h to eliminate the uninfected cells before collecting the whole cell lysates (WCLs) for the subsequent biochemical assays.

Suppression or overexpression techniques. Either lentiviral or retroviral infections (viral transductions) were performed as follows: 6×10^5 HEK 293T cells were seeded in 60-mm dishes and cotransfected the next day with each lentivirus or retrovirus vector, along with helper plasmids (i.e., gag-pol and VSV-G were used for lentiviral infections). Media with progeny virus from transfected HEK 293T cells was collected every 24 h for 2 d, and then filtered with 0.45-μm filters (Millipore) and freshly used to transduce 293T, HeLa, HMVEC, and BCPAP cells overnight in the presence of 8 μg/ml Polybrene (Sigma-Aldrich). Finally, stable transduced cells were treated with 2.5 μg/ml blasticidin or 1–2 μg/ml puromycin (Sigma-Aldrich) for selection. Gene or protein knockdown or overexpression in the transduced cells was confirmed by real-time RT-PCR and Western blot analysis. All assays were performed in triplicate.

Antibodies and reagents. Anti c-Myc, polyclonal anti-HA, anti-CKIδ (H-60), anti-CKIα, anti-Cullin 1, anti–FLK-1 (A-3) AC, anti–β-TRCP, anti-CCM3, and anti–human VEGF-A antibodies were purchased from Santa Cruz Biotechnology, Inc. Anti-Cullin5 was from Bethyl Laboratories, Inc., and anti-Cullin4 (2699S) and anti–β-TRCP (D13F10) antibodies were purchased from Cell Signaling Technology. Anti-CKIε antibody was purchased from BD. Anti-tubulin, polyclonal anti-FLAG, monoclonal anti-FLAG, peroxidase-conjugated anti–mouse secondary antibody, peroxidase-conjugated anti–rabbit secondary antibody, anti-Flag agarose beads, and anti-HA agarose beads were purchased from Sigma-Aldrich. Monoclonal anti-HA antibody was purchased from Covance. Anti-GFP antibody was obtained from Invitrogen. Anti-VEGFR1, anti-VEGFR2, anti-VEGFR3, anti–phospho-VEGFR2-1175, anti–phospho-AKT (ser473), anti–total-AKT1, anti-pERK1/2, and anti–total-ERK1/2 antibodies were purchased from Cell Signaling Technology. Sorafenib was purchased from Enzo Life Sciences and VEGF-A was obtained from Dr. Lawler's laboratory.

Immunoblots and immunoprecipitation. Cells were lysed in EBC (50 mM Tris, pH 8.0, 120 mM NaCl, and 0.5% NP-40) buffer supplemented with protease inhibitors (Complete Mini; Roche) and phosphatase inhibitors (phosphatase inhibitor cocktail set I and II; EMD). The protein concentrations of the lysates were measured using a protein assay reagent (Bio-Rad Laboratories) on a DU-800 spectrophotometer (Beckman Coulter). The lysates were then resolved by SDS-PAGE and immunoblotted with the indicated antibodies. For immunoprecipitation, 20 h after transfection, cells were treated with 10 μM MG132 overnight before harvesting for immunoprecipitation procedures. 800 μg of protein lysates were incubated with the appropriate antibody (1–2 μg) overnight at 4°C, followed by the addition of carrier beads. Immunocomplexes were washed five times with NETN buffer (20 mM Tris, pH 8.0, 100 mM NaCl, 1 mM EDTA, and 0.5% NP-40) before being resolved by SDS-PAGE and immunoblotted with indicated antibodies.

Protein degradation analysis. Cells were plated into 6-cm tissue culture dishes 20 h before transfection. When cells reached an appropriate confluence, they were transfected with 2.0 μg HA-VEGFR2, along with 1.0 μg Flag-β-TRCP1 and 0.1 μg of a plasmid encoding GFP as an internal control, in the presence or absence of 0.4 μg Myc-CKIδ. For half-life studies, 20 μg/ml cycloheximide (CHX; Sigma-Aldrich) was added to the medium 40 h after transfection. At various time points thereafter, cells were lysed and protein concentrations were measured. 30 μg of the indicated WCLs were separated by SDS-PAGE and protein abundances were measured by immunoblot analysis.

Real-time RT–PCR analysis. RNA was extracted with an RNeasy mini kit (QIAGEN), and the reverse transcription reaction was performed with the ABI TaqMan Reverse Transcription Reagents (N808-0234). After mixing the resulting template with VEGFR2 (Hs00911700_m1), β-TRCP1 (Hs001182707_m1), or β-TRCP2 (Hs00362667_m1) primers and TaqMan Fast Universal PCR Master Mix (4352042; Applied Biosystems), the real-time RT-PCR reaction was performed with the ABI-7500 Fast Real-time PCR system (Applied Biosystems). VEGF-A copies number/10^6 18S were assessed by absolute quantification using real-time RT-PCR (Shih and Smith, 2005) using the VEGF-A and 18S primer sequences provided by the Multigene Transcriptional Profiling Core Facility (Center for Vascular Biology Research, Beth Israel Deaconess Medical Center, Harvard Medical School, Boston, MA).

VEGFR2 binding assays. Binding to immobilized GST proteins was performed as described previously (Wei et al., 2004). Where indicated, the GST-VEGFR2 proteins were incubated with CKIδ in the presence of ATP for 1 h before the binding assays.

In vitro kinase assay. CKIδ was purchased from New England Biolabs, Inc. The CKI in vitro kinase assays were performed according to the manufacturer's instructions (New England Biolabs, Inc.). In brief, 5 μg of indicated GST fusion proteins were incubated with purified active CKIδ in the presence of 5 μCi γ-[^{32}P]ATP and 200 μM cold ATP in the CKI reaction buffer for 30 min. The reaction was stopped by the addition of SDS-containing lysis buffer, resolved on SDS-PAGE, and detected by autoradiography (Inuzuka et al., 2010).

In vitro ubiquitination assay. The in vitro ubiquitination assays were performed as described previously (Jin et al., 2005). To purify $SCF^{β\text{-}TRCP1}$ complex, 293T cells were transfected with vectors encoding GST–β-TRCP1, Myc–Cul-1, Myc-Skp1, and HA-Rbx1. The $SCF^{β\text{-}TRCP1}$ (E3) complexes were purified from the WCLs using GST-agarose beads. Before the in vitro ubiquitination assay, indicated GST-VEGFR2 proteins were incubated with purified, recombinant active CKIδ in the presence of ATP (with kinase reaction buffer as a negative control) at 30°C for 30 min. Afterward, the kinase reaction products were incubated with purified $SCF^{β\text{-}TRCP1}$ (E3) complexes in the presence of purified, recombinant active E1, E2 (UbcH5a and UbcH3), ATP, and ubiquitin at 30°C for 45 min. The reactions were stopped by the addition of SDS-PAGE sample buffer and the reaction products were resolved by SDS-PAGE and probed with the indicated antibodies (Inuzuka et al., 2010).

Cell migration assay and trans-well co-culture system. Migration assays were performed according to manufacturer's instructions using chambers (Corning) that did not contain Matrigel. In brief, shGFP- or shβ-TRCP cells (2.5×10^4 HMVECs/0.5 ml) without serum were seeded into the insert. The bottom face of the filters (with 8-μm pore) were coated with type I collagen. 5% FBS in growth medium was added into the wells as a chemoattractant. In brief, these trans-wells/chambers were used to study the effect of β-TRCP knockdown on the migration of transduced HMVECs in the presence or absence of 30–100 ng/ml VEGF-A. The migration assay was performed for 5–18 h in culture and then inserts were fixed in methanol for 2 min, stained with Giemsa for 30 min, washed in distilled water, and air dried. Additionally, shGFP or shVEGFR2 BCPAP cells were grown in 10% serum for 24 h, and then 1×10^5 cells/0.5 ml were seeded into the insert (in the presence or absence of 100 ng/ml human VEGF-A, added into the insert along with the cells) of the transwell and 5% FBS in growth medium was added into the wells as chemoattractant. Migration assay was run for ∼4 h. BCPAP cells (EV or HA-β-TRCP1) were cultured (2×10^4 cells/0.5 ml/insert of transwell) were grown for 24 h with low serum (2%) and then serum-free overnight before migration assay. 200 ng/ml VEGF-A was used as chemoattractant in the well. Migration assay was run for ∼18 h.

We also generated a trans-well cell co-culture system (Fig. 9 A). BCPAP cells (EV or HA-β-TRCP1) were cultured (2×10^4 cells/well) in 24-well plates. HMVECs (5×10^4 cells/0.5 ml) were placed in inserts and placed on top of each well in serum-free medium. Therefore, these two types of cells were separated by the insert membrane. The secreted VEGF-A from the BCPAP cells (which were grown in the absence of serum) served as chemoattractant to induce migration of HMVECs (Fig. 9 A–C). The assay was conducted in the presence or absence of 5–10 μg human VEGF-A antibody for ∼44 h, and the migrated HMVECs were photographed and quantified as described. In all assays, migrated cells were counted (number of cells/field or number of cells/well) using a 10 or 20× objective, and four fields were chosen per well with two well per each condition. Furthermore, migrated cells were also photographed using a camera attached to the microscope.

In vitro angiogenesis assay. The in vitro angiogenesis assays (tube formation assays) were performed as previously described (Ponce, 2001). In brief, control shGFP and shβ-TRCP HMVECs (4×10^4/0.5 ml) in EGM medium containing 2% serum were seeded on Matrigel (BD) and treated with or without 100 ng/ml VEGF-A. After 5 h of incubation, cells were photographed using the camera attached to the microscope. The number of tubes was counted using a 10 or 20× objective and four fields were chosen per well with two wells per each condition.

Zebrafish MO knockdown experiments. Zebrafish were maintained according to Institutional Animal Care and Use Committee (IACUC-BIDMC) protocols. The MO sequences were used to target Fbxw11a (5′-AGGTTTTGTCCTCCATCTCCGTCTC-3′; or the splice form, 5′-GAAATACAACACACACCTTGAACAC-3′) and Fbxw11b (5′-ATTGTTGTTCTAGCTGAATCCAACC-3′; or the splice form, 5′-AAGAGCACCCAAACACTTACCATCT-3′). Control and knockdown MOs specifically targeted to β-TRCP2 were injected into wild-type or endothelial reporter (Kdrl:EGFP and fli1a:EGFP) zebrafish at the one cell stage (three independent replicate experiments were performed). At 72 h after fertilization, viability counts were enumerated and/or embryos were imaged by fluorescence microscopy using a microscope (Discovery; Carl Zeiss) to assess alterations in vascular development in two independent zebrafish reporter lines: Kdrl:EGFP (Cross et al., 2003) and fli1a:EGFP (Lawson and Weinstein, 2002). In situ hybridization and RT-PCR were conducted using standard zebrafish protocols (www.zfin.org). The following RT-PCR primers were used: fbxw11a forward 5′-ACAAAACCCTGGAGCTGATG-3′, and reverse 5′-GTCCAGGAACGACAGGATGT-3′; and fbxw11b forward 5′-CATTTTCACTGCGAGTTTCG-3′, and reverse 5′-TCAAAGAGCTGGATGCACAC-3′. Anti-VEGFR2 antibody (Abcam) was used to detect endogenous VEGFR2 in zebrafish. This antibody was raised with synthetic nonphosphopeptide derived from human VEGFR2 around the phosphorylation site of tyrosine 1059 (P-D-YP-V-R), a region which shares a high degree of homology with the zebrafish VEGFR2 protein.

Cell viability assay. Human thyroid cancer cell lines (1×10^4 cells/well) were cultured in medium containing 0.5% serum and plated in a 96-well sterile culture plate. Cells were treated with or without various concentrations of sorafenib for 48 h. Cell viability was measured using the CellTiter-Glo Luminescent Cell Viability assay kit according to the manufacturer's instructions (Promega).

ELISA. BCPAP, EV-BCPAP, HA-β-TRCP1-BCPAP, SW1736, and 8505C thyroid cancer cells were cultured in 6-cm dishes with serum-free medium overnight. The next day, the medium was collected and secreted VEGF-A protein levels were determined by ELISA kit (R&D Systems) according to the manufacturer's instructions.

Flow cytometry analysis. sh-GFP or sh-β-TRCP transduced HMVECs were serum starved overnight and then collected, fixed with 75% ethanol, and stained with propidium iodide for flow cytometry analysis according to Nucera et al., (2010) using FACS (BD) to assess sub-G1 cell populations.

Histological and immunohistochemical analysis. All tissue specimens were fixed with 10% buffered formalin phosphate and embedded in paraffin

blocks. Histopathology evaluation was performed by an endocrine pathologist (P.M. Sadow) on hematoxylin and eosin (H&E)–stained tissue sections of 15 human thyroid carcinomas under the approval of Massachusetts General Hospital IRB committee (P.M. Sadow, 2011P000013). These were visualized with a microscope (BX 41; Olympus) and a camera (Q COLOR 5 photo; Olympus). 4-µm-thick sections of 10 formalin-fixed human thyroid carcinomas with squamous metaplasia foci (6 classical PTC, 1 PTC tall cell variant, 1 PTC diffuse sclerosing variant, 1 squamous cell carcinoma, and 1 poorly differentiated thyroid carcinoma) classified according to the World Health Organization (for squamous metaplasia features read Kleer et al., 2000). Tumor size was >0.4 cm (range: 0.4–4.5 cm; mean: 1.6 cm). 4 out of 10 thyroid carcinomas showed extra thyroidal extension, 4 out of 10 thyroid carcinomas showed lymphovascular invasion, and 4 out of 10 thyroid carcinomas showed neck lymph nodes metastasis (Table S1). These thyroid tumor tissues were used for immunohistochemical (IHC) procedures. After baking overnight at 37°C, deparaffinization with xylene/ethanol and rehydration were performed. IHC was performed using the β-TRCP (Santa Cruz Biotechnology, Inc.), VEGFR2 (2479; Cell Signaling Technology), VEGF-A (C1; Santa Cruz Biotechnology, Inc.), D2-40 (marker of lymphatic vessels; Covance), and CD31 (marker of endothelial cells; M20; Abcam) primary antibodies. The sections, treated in a pressure cooker for antigen retrieval (Biocare Medical), were incubated at 123°C in Citrate buffer (Target Retrieval Solution; DAKO), cooled, and washed with PBS. Antigen retrieval was performed for 60 min at RT. The primary antibody was detected using a biotin-free secondary antibody (K4011; Envision system; DAKO) and incubated for 30 min. All incubations were performed in a humid chamber at room temperature. Slides were rinsed with PBS between incubations. Sections were developed using 3,3′-diaminobenzidine (DAB; Sigma-Aldrich) as a substrate and were counterstained with Mayer's Hematoxylin. The immunohistochemical markers were assessed semi-quantitatively using the following scoring method: 0, negative; 1+, 1–10% positive cells (low expression); 2+, 11–50% positive cells (moderate expression); and 3+, >50% positive cells (high expression).

Statistical analysis. Results were expressed as mean ± SD. Statistical comparisons were made using an unpaired Student's *t* test and one way ANOVA (Excel; Microsoft). Densitometry analysis was performed using ImageJ software (National Institutes of Health) and values were normalized to tubulin. Differences were considered statistically significant when $P < 0.05$.

Online supplemental material. Fig. S1 lists the DSG(XX)S phosphodegron sequences in VEGFR2 recognized by β-TRCP, as well as potential and predicted CKI-mediated phosphorylation sites in VEGFR2. Fig. S2 presents zebrafish embryo viability data after treatment with MOs that target β-TRCP2. Fig. S3 lists the β-TRCP–recognizable DSG-like canonical degron consensus in VEGF-A among various species. Table S1 lists the β-TRCP1 protein expression levels and angiogenesis markers in human thyroid cancers. Online supplemental material is available at http://www.jem.org/cgi/content/full/jem.20112446/DC1.

We thank Rong Shao (Veterinary and Animal Sciences, University of Massachusetts, Amherst, MA) for providing the HMVEC line, and Jacques Huot and Francois Houle (Laval University Cancer Research Center, Québec, Canada) for the pIRES-VEGFR2-HA construct. We thank Harold F. Dvorak, Alex Toker, and Issac Rabinovitz for constructive suggestions. We thank Mark A Duquette, Shideh Khazerounian, Mei Zheng, and Nina Hu for technical assistance.

W. Wei is a DOD Prostate Research Program New Investigator and American Cancer Society Scholar. This work was supported in part by the National Institutes of Health (NIH) grants to W. Wei (GM089763 and GM094777) and J. Lawler (CA130895). S. Shaik is supported by a NRSA T-32 training grant, H. Inuzuka was awarded a K01 grant (AG041218) from NIH, and H. Fukushima is supported by a JSPS Postdoctoral Fellowship. C. Nucera was the recipient of a Ph.D. fellowship from the Italian Ministry of Education, Universities and Research (MIUR). C. Nucera is also funded by the American Thyroid Association for a Thyroid Cancer Grant.

The authors have no conflicting financial interests.

Submitted: 16 November 2011
Accepted: 4 June 2012

REFERENCES

Ahmad, I., S. Balasubramanian, C.B. Del Debbio, S. Parameswaran, A.R. Katz, C. Toris, and R.N. Fariss. 2011. Regulation of ocular angiogenesis by Notch signaling: implications in neovascular age-related macular degeneration. *Invest. Ophthalmol. Vis. Sci.* 52:2868–2878. http://dx.doi.org/10.1167/iovs.10-6608

Alitalo, K., and P. Carmeliet. 2002. Molecular mechanisms of lymphangiogenesis in health and disease. *Cancer Cell.* 1:219–227. http://dx.doi.org/10.1016/S1535-6108(02)00051-X

Al Sabti, H. 2007. Therapeutic angiogenesis in cardiovascular disease. *J. Cardiothorac. Surg.* 2:49. http://dx.doi.org/10.1186/1749-8090-2-49

Baudin, E., and M. Schlumberger. 2007. New therapeutic approaches for metastatic thyroid carcinoma. *Lancet Oncol.* 8:148–156. http://dx.doi.org/10.1016/S1470-2045(07)70034-7

Bergers, G., and L.E. Benjamin. 2003. Tumorigenesis and the angiogenic switch. *Nat. Rev. Cancer.* 3:401–410. http://dx.doi.org/10.1038/nrc1093

Brown, L.F., M. Detmar, K. Claffey, J.A. Nagy, D. Feng, A.M. Dvorak, and H.F. Dvorak. 1997. Vascular permeability factor/vascular endothelial growth factor: a multifunctional angiogenic cytokine. *EXS.* 79:233–269.

Bunone, G., P. Vigneri, L. Mariani, S. Butó, P. Collini, S. Pilotti, M.A. Pierotti, and I. Bongarzone. 1999. Expression of angiogenesis stimulators and inhibitors in human thyroid tumors and correlation with clinical pathological features. *Am. J. Pathol.* 155:1967–1976. http://dx.doi.org/10.1016/S0002-9440(10)65515-0

Busino, L., M. Donzelli, M. Chiesa, D. Guardavaccaro, D. Ganoth, N.V. Dorrello, A. Hershko, M. Pagano, and G.F. Draetta. 2003. Degradation of Cdc25A by beta-TrCP during S phase and in response to DNA damage. *Nature.* 426:87–91. http://dx.doi.org/10.1038/nature02082

Cabanillas, M.E., S.G. Waguespack, Y. Bronstein, M.D. Williams, L. Feng, M. Hernandez, A. Lopez, S.I. Sherman, and N.L. Busaidy. 2010. Treatment with tyrosine kinase inhibitors for patients with differentiated thyroid cancer: the M. D. Anderson experience. *J. Clin. Endocrinol. Metab.* 95:2588–2595. http://dx.doi.org/10.1210/jc.2009-1923

Cardozo, T., and M. Pagano. 2004. The SCF ubiquitin ligase: insights into a molecular machine. *Nat. Rev. Mol. Cell Biol.* 5:739–751. http://dx.doi.org/10.1038/nrm1471

Chakravarty, D., E. Santos, M. Ryder, J.A. Knauf, X.H. Liao, B.L. West, G. Bollag, R. Kolesnick, T.H. Thin, N. Rosen, et al. 2011. Small-molecule MAPK inhibitors restore radioiodine incorporation in mouse thyroid cancers with conditional BRAF activation. *J. Clin. Invest.* 121:4700–4711. http://dx.doi.org/10.1172/JCI46382

Ciechanover, A., A. Orian, and A.L. Schwartz. 2000. Ubiquitin-mediated proteolysis: biological regulation via destruction. *Bioessays.* 22:442–451. http://dx.doi.org/10.1002/(SICI)1521-1878(200005)22:5<442::AID-BIES6>3.0.CO;2-Q

Cohen, E.E., L.S. Rosen, E.E. Vokes, M.S. Kies, A.A. Forastiere, F.P. Worden, M.A. Kane, E. Sherman, S. Kim, P. Bycott, et al. 2008. Axitinib is an active treatment for all histologic subtypes of advanced thyroid cancer: results from a phase II study. *J. Clin. Oncol.* 26:4708–4713. http://dx.doi.org/10.1200/JCO.2007.15.9566

Cross, L.M., M.A. Cook, S. Lin, J.N. Chen, and A.L. Rubinstein. 2003. Rapid analysis of angiogenesis drugs in a live fluorescent zebrafish assay. *Arterioscler. Thromb. Vasc. Biol.* 23:911–912. http://dx.doi.org/10.1161/01.ATV.0000068685.72914.7E

Davies, L., and H.G. Welch. 2006. Increasing incidence of thyroid cancer in the United States, 1973-2002. *JAMA.* 295:2164–2167. http://dx.doi.org/10.1001/jama.295.18.2164

Dvorak, H.F. 2003. Rous-Whipple Award Lecture. How tumors make bad blood vessels and stroma. *Am. J. Pathol.* 162:1747–1757. http://dx.doi.org/10.1016/S0002-9440(10)64309-X

Fabien, N., A. Fusco, M. Santoro, Y. Barbier, P.M. Dubois, and C. Paulin. 1994. Description of a human papillary thyroid carcinoma cell line. Morphologic study and expression of tumoral markers. *Cancer.* 73:2206–2212. http://dx.doi.org/10.1002/1097-0142(19940415)73:8<2206::AID-CNCR2820730828>3.0.CO;2-M

Ferrara, N. 1999. Molecular and biological properties of vascular endothelial growth factor. *J. Mol. Med.* 77:527–543. http://dx.doi.org/10.1007/s001099900019

Folkman, J. 1971. Tumor angiogenesis: therapeutic implications. *N. Engl. J. Med.* 285:1182–1186. http://dx.doi.org/10.1056/NEJM197111182852108

Folkman, J. 2007. Angiogenesis: an organizing principle for drug discovery? *Nat. Rev. Drug Discov.* 6:273–286. http://dx.doi.org/10.1038/nrd2115

Fong, T.A., L.K. Shawver, L. Sun, C. Tang, H. App, T.J. Powell, Y.H. Kim, R. Schreck, X. Wang, W. Risau, et al. 1999. SU5416 is a potent and selective inhibitor of the vascular endothelial growth factor receptor (Flk-1/KDR) that inhibits tyrosine kinase catalysis, tumor vascularization, and growth of multiple tumor types. *Cancer Res.* 59:99–106.

Frescas, D., and M. Pagano. 2008. Deregulated proteolysis by the F-box proteins SKP2 and beta-TrCP: tipping the scales of cancer. *Nat. Rev. Cancer.* 8:438–449. http://dx.doi.org/10.1038/nrc2396

Gupta-Abramson, V., A.B. Troxel, A. Nellore, K. Puttaswamy, M. Redlinger, K. Ransone, S.J. Mandel, K.T. Flaherty, L.A. Loevner, P.J. O'Dwyer, and M.S. Brose. 2008. Phase II trial of sorafenib in advanced thyroid cancer. *J. Clin. Oncol.* 26:4714–4719. http://dx.doi.org/10.1200/JCO.2008.16.3279

Habeck, H., J. Odenthal, B. Walderich, H. Maischein, and S. Schulte-Merker; Tübingen 2000 screen consortium. 2002. Analysis of a zebrafish VEGF receptor mutant reveals specific disruption of angiogenesis. *Curr. Biol.* 12:1405–1412. http://dx.doi.org/10.1016/S0960-9822(02)01044-8

He, Y., H. Zhang, L. Yu, M. Gunel, T.J. Boggon, H. Chen, and W. Min. 2010. Stabilization of VEGFR2 signaling by cerebral cavernous malformation 3 is critical for vascular development. *Sci. Signal.* 3:ra26. http://dx.doi.org/10.1126/scisignal.2000722

Inuzuka, H., A. Tseng, D. Gao, B. Zhai, Q. Zhang, S. Shaik, L. Wan, X.L. Ang, C. Mock, H. Yin, et al. 2010. Phosphorylation by casein kinase I promotes the turnover of the Mdm2 oncoprotein via the SCF(beta-TRCP) ubiquitin ligase. *Cancer Cell.* 18:147–159. http://dx.doi.org/10.1016/j.ccr.2010.06.015

Jin, J., T. Shirogane, L. Xu, G. Nalepa, J. Qin, S.J. Elledge, and J.W. Harper. 2003. SCFbeta-TRCP links Chk1 signaling to degradation of the Cdc25A protein phosphatase. *Genes Dev.* 17:3062–3074. http://dx.doi.org/10.1101/gad.1157503

Jin, J., X.L. Ang, T. Shirogane, and J. Wade Harper. 2005. Identification of substrates for F-box proteins. *Methods Enzymol.* 399:287–309. http://dx.doi.org/10.1016/S0076-6879(05)99020-4

Kanarek, N., E. Horwitz, I. Mayan, M. Leshets, G. Cojocaru, M. Davis, B.Z. Tsuberi, E. Pikarsky, M. Pagano, and Y. Ben-Neriah. 2010. Spermatogenesis rescue in a mouse deficient for the ubiquitin ligase SCFbeta-TrCP by single substrate depletion. *Genes Dev.* 24:470–477. http://dx.doi.org/10.1101/gad.551610

Keefe, S.M., M.A. Cohen, and M.S. Brose. 2010. Targeting vascular endothelial growth factor receptor in thyroid cancer: the intracellular and extracellular implications. *Clin. Cancer Res.* 16:778–783. http://dx.doi.org/10.1158/1078-0432.CCR-08-2743

Khan, T.A., F.W. Sellke, and R.J. Laham. 2002. Therapeutic angiogenesis for coronary artery disease. *Curr. Treat. Options Cardiovasc. Med.* 4:65–74. http://dx.doi.org/10.1007/s11936-002-0027-z

Khurana, R., M. Simons, J.F. Martin, and I.C. Zachary. 2005. Role of angiogenesis in cardiovascular disease: a critical appraisal. *Circulation.* 112:1813–1824. http://dx.doi.org/10.1161/CIRCULATIONAHA.105.535294

Kleer, C.G., T.J. Giordano, and M.J. Merino. 2000. Squamous cell carcinoma of the thyroid: an aggressive tumor associated with tall cell variant of papillary thyroid carcinoma. *Mod. Pathol.* 13:742–746. http://dx.doi.org/10.1038/modpathol.3880129

Kloos, R.T., M.D. Ringel, M.V. Knopp, N.C. Hall, M. King, R. Stevens, J. Liang, P.E. Wakely Jr., V.V. Vasko, M. Saji, et al. 2009. Phase II trial of sorafenib in metastatic thyroid cancer. *J. Clin. Oncol.* 27:1675–1684. http://dx.doi.org/10.1200/JCO.2008.18.2717

Knauf, J.A., and J.A. Fagin. 2009. Role of MAPK pathway oncoproteins in thyroid cancer pathogenesis and as drug targets. *Curr. Opin. Cell Biol.* 21:296–303. http://dx.doi.org/10.1016/j.ceb.2009.01.013

Kranz, A., T. Mattfeldt, and J. Waltenberger. 1999. Molecular mediators of tumor angiogenesis: enhanced expression and activation of vascular endothelial growth factor receptor KDR in primary breast cancer. *Int. J. Cancer.* 84:293–298. http://dx.doi.org/10.1002/(SICI)1097-0215(19990621)84:3<293::AID-IJC16>3.0.CO;2-T

Lam, E.T., M.D. Ringel, R.T. Kloos, T.W. Prior, M.V. Knopp, J. Liang, S. Sammet, N.C. Hall, P.E. Wakely Jr., V.V. Vasko, et al. 2010. Phase II clinical trial of sorafenib in metastatic medullary thyroid cancer. *J. Clin. Oncol.* 28:2323–2330. http://dx.doi.org/10.1200/JCO.2009.25.0068

Lawson, N.D., and B.M. Weinstein. 2002. In vivo imaging of embryonic vascular development using transgenic zebrafish. *Dev. Biol.* 248:307–318. http://dx.doi.org/10.1006/dbio.2002.0711

Leenhardt, L., P. Grosclaude, and L. Chérié-Challine; Thyroid Cancer Committee. 2004. Increased incidence of thyroid carcinoma in france: a true epidemic or thyroid nodule management effects? Report from the French Thyroid Cancer Committee. *Thyroid.* 14:1056–1060. http://dx.doi.org/10.1089/thy.2004.14.1056

Li, Y., C.V. Clevenger, N. Minkovsky, K.G. Kumar, P.N. Raghunath, J.E. Tomaszewski, V.S. Spiegelman, and S.Y. Fuchs. 2006. Stabilization of prolactin receptor in breast cancer cells. *Oncogene.* 25:1896–1902. http://dx.doi.org/10.1038/sj.onc.1209214

Liu, C., Y. Kato, Z. Zhang, V.M. Do, B.A. Yankner, and X. He. 1999. beta-Trcp couples beta-catenin phosphorylation-degradation and regulates Xenopus axis formation. *Proc. Natl. Acad. Sci. USA.* 96:6273–6278. http://dx.doi.org/10.1073/pnas.96.11.6273

Liu, C., Y. Li, M. Semenov, C. Han, G.H. Baeg, Y. Tan, Z. Zhang, X. Lin, and X. He. 2002. Control of beta-catenin phosphorylation/degradation by a dual-kinase mechanism. *Cell.* 108:837–847. http://dx.doi.org/10.1016/S0092-8674(02)00685-2

Liu, D., J. Xing, B. Trink, and M. Xing. 2010. BRAF mutation-selective inhibition of thyroid cancer cells by the novel MEK inhibitor RDEA119 and genetic-potentiated synergism with the mTOR inhibitor temsirolimus. *Int. J. Cancer.* 127:2965–2973. http://dx.doi.org/10.1002/ijc.25304

Meyer, R.D., A.J. Singh, and N. Rahimi. 2004. The carboxyl terminus controls ligand-dependent activation of VEGFR-2 and its signaling. *J. Biol. Chem.* 279:735–742. http://dx.doi.org/10.1074/jbc.M305575200

Meyer, R.D., S. Srinivasan, A.J. Singh, J.E. Mahoney, K.R. Gharahassanlou, and N. Rahimi. 2011. PEST motif serine and tyrosine phosphorylation controls vascular endothelial growth factor receptor 2 stability and downregulation. *Mol. Cell. Biol.* 31:2010–2025. http://dx.doi.org/10.1128/MCB.01006-10

Nasevicius, A., J. Larson, and S.C. Ekker. 2000. Distinct requirements for zebrafish angiogenesis revealed by a VEGF-A morphant. *Yeast.* 17:294–301. http://dx.doi.org/10.1002/1097-0061(200012)17:4<294::AID-YEA54>3.0.CO;2-5

Nucera, C., M. Goldfarb, R. Hodin, and S. Parangi. 2009. Role of B-Raf(V600E) in differentiated thyroid cancer and preclinical validation of compounds against B-Raf(V600E). *Biochim. Biophys. Acta.* 1795:152–161.

Nucera, C., A. Porrello, Z.A. Antonello, M. Mekel, M.A. Nehs, T.J. Giordano, D. Gerald, L.E. Benjamin, C. Priolo, E. Puxeddu, et al. 2010. B-Raf(V600E) and thrombospondin-1 promote thyroid cancer progression. *Proc. Natl. Acad. Sci. USA.* 107:10649–10654. http://dx.doi.org/10.1073/pnas.1004934107

Papetti, M., and I.M. Herman. 2002. Mechanisms of normal and tumor-derived angiogenesis. *Am. J. Physiol. Cell Physiol.* 282:C947–C970.

Petroski, M.D., and R.J. Deshaies. 2005. Function and regulation of cullin-RING ubiquitin ligases. *Nat. Rev. Mol. Cell Biol.* 6:9–20. http://dx.doi.org/10.1038/nrm1547

Ponce, M.L. 2001. In vitro matrigel angiogenesis assays. *Methods Mol. Med.* 46:205–209.

Ringel, M.D. 2011. Metastatic dormancy and progression in thyroid cancer: targeting cells in the metastatic frontier. *Thyroid.* 21:487–492. http://dx.doi.org/10.1089/thy.2011.2121

Rodríguez-Antona, C., J. Pallares, C. Montero-Conde, L. Inglada-Pérez, E. Castelblanco, I. Landa, S. Leskelä, L.J. Leandro-García, E. López-Jiménez, R. Letón, et al. 2010. Overexpression and activation of EGFR and VEGFR2 in medullary thyroid carcinomas is related to metastasis. *Endocr. Relat. Cancer.* 17:7–16. http://dx.doi.org/10.1677/ERC-08-0304

Schlessinger, J. 2000. Cell signaling by receptor tyrosine kinases. *Cell.* 103:211–225. http://dx.doi.org/10.1016/S0092-8674(00)00114-8

Senger, D.R., S.J. Galli, A.M. Dvorak, C.A. Perruzzi, V.S. Harvey, and H.F. Dvorak. 1983. Tumor cells secrete a vascular permeability factor that promotes accumulation of ascites fluid. *Science*. 219:983–985. http://dx.doi.org/10.1126/science.6823562

Senger, D.R., C.A. Perruzzi, J. Feder, and H.F. Dvorak. 1986. A highly conserved vascular permeability factor secreted by a variety of human and rodent tumor cell lines. *Cancer Res.* 46:5629–5632.

Seto, T., M. Higashiyama, H. Funai, F. Imamura, K. Uematsu, N. Seki, K. Eguchi, T. Yamanaka, and Y. Ichinose. 2006. Prognostic value of expression of vascular endothelial growth factor and its flt-1 and KDR receptors in stage I non-small-cell lung cancer. *Lung Cancer.* 53:91–96. http://dx.doi.org/10.1016/j.lungcan.2006.02.009

Shalaby, F., J. Rossant, T.P. Yamaguchi, M. Gertsenstein, X.F. Wu, M.L. Breitman, and A.C. Schuh. 1995. Failure of blood-island formation and vasculogenesis in Flk-1-deficient mice. *Nature*. 376:62–66. http://dx.doi.org/10.1038/376062a0

Shao, R., and X. Guo. 2004. Human microvascular endothelial cells immortalized with human telomerase catalytic protein: a model for the study of in vitro angiogenesis. *Biochem. Biophys. Res. Commun.* 321:788–794. http://dx.doi.org/10.1016/j.bbrc.2004.07.033

Sherman, S.I. 2011. Targeted therapies for thyroid tumors. *Mod. Pathol.* 24(Suppl 2):S44–S52. http://dx.doi.org/10.1038/modpathol.2010.165

Shibuya, M., and L. Claesson-Welsh. 2006. Signal transduction by VEGF receptors in regulation of angiogenesis and lymphangiogenesis. *Exp. Cell Res.* 312:549–560. http://dx.doi.org/10.1016/j.yexcr.2005.11.012

Shih, S.C., and L.E. Smith. 2005. Quantitative multi-gene transcriptional profiling using real-time PCR with a master template. *Exp. Mol. Pathol.* 79:14–22. http://dx.doi.org/10.1016/j.yexmp.2005.03.004

Shirogane, T., J. Jin, X.L. Ang, and J.W. Harper. 2005. SCFbeta-TRCP controls clock-dependent transcription via casein kinase 1-dependent degradation of the mammalian period-1 (Per1) protein. *J. Biol. Chem.* 280:26863–26872. http://dx.doi.org/10.1074/jbc.M502862200

Singh, A.J., R.D. Meyer, H. Band, and N. Rahimi. 2005. The carboxyl terminus of VEGFR-2 is required for PKC-mediated down-regulation. *Mol. Biol. Cell.* 16:2106–2118. http://dx.doi.org/10.1091/mbc.E04-08-0749

Takahashi, Y., Y. Kitadai, C.D. Bucana, K.R. Cleary, and L.M. Ellis. 1995. Expression of vascular endothelial growth factor and its receptor, KDR, correlates with vascularity, metastasis, and proliferation of human colon cancer. *Cancer Res.* 55:3964–3968.

Tonnesen, M.G., X. Feng, and R.A. Clark. 2000. Angiogenesis in wound healing. *J. Investig. Dermatol. Symp. Proc.* 5:40–46. http://dx.doi.org/10.1046/j.1087-0024.2000.00014.x

Ungvari, Z., G. Kaley, R. de Cabo, W.E. Sonntag, and A. Csiszar. 2010. Mechanisms of vascular aging: new perspectives. *J. Gerontol. A Biol. Sci. Med. Sci.* 65A:1028–1041. http://dx.doi.org/10.1093/gerona/glq113

Vieira, J.M., S.C. Santos, C. Espadinha, I. Correia, T. Vag, C. Casalou, B.M. Cavaco, A.L. Catarino, S. Dias, and V. Leite. 2005. Expression of vascular endothelial growth factor (VEGF) and its receptors in thyroid carcinomas of follicular origin: a potential autocrine loop. *Eur. J. Endocrinol.* 153:701–709. http://dx.doi.org/10.1530/eje.1.02009

Walvekar, R.R., S.V. Kane, and A.K. D'Cruz. 2006. Collision tumor of the thyroid: follicular variant of papillary carcinoma and squamous carcinoma. *World J. Surg. Oncol.* 4:65. http://dx.doi.org/10.1186/1477-7819-4-65

Watanabe, N., H. Arai, Y. Nishihara, M. Taniguchi, N. Watanabe, T. Hunter, and H. Osada. 2004. M-phase kinases induce phospho-dependent ubiquitination of somatic Wee1 by SCFbeta-TrCP. *Proc. Natl. Acad. Sci. USA.* 101:4419–4424. http://dx.doi.org/10.1073/pnas.0307700101

Wei, W., N.G. Ayad, Y. Wan, G.J. Zhang, M.W. Kirschner, and W.G. Kaelin Jr. 2004. Degradation of the SCF component Skp2 in cell-cycle phase G1 by the anaphase-promoting complex. *Nature*. 428:194–198. http://dx.doi.org/10.1038/nature02381

Weinstein, B. 2002. Vascular cell biology in vivo: a new piscine paradigm? *Trends Cell Biol.* 12:439–445. http://dx.doi.org/10.1016/S0962-8924(02)02358-9

Weinstein, I.B., and A.K. Joe. 2006. Mechanisms of disease: Oncogene addiction—a rationale for molecular targeting in cancer therapy. *Nat. Clin. Pract. Oncol.* 3:448–457. http://dx.doi.org/10.1038/ncponc0558

Wu, G., G. Xu, B.A. Schulman, P.D. Jeffrey, J.W. Harper, and N.P. Pavletich. 2003. Structure of a beta-TrCP1-Skp1-beta-catenin complex: destruction motif binding and lysine specificity of the SCF(beta-TrCP1) ubiquitin ligase. *Mol. Cell.* 11:1445–1456. http://dx.doi.org/10.1016/S1097-2765(03)00234-X

Zhang, H., J. Wu, L. Meng, and C.C. Shou. 2002. Expression of vascular endothelial growth factor and its receptors KDR and Flt-1 in gastric cancer cells. *World J. Gastroenterol.* 8:994–998.